

AN ABSTRACT OF THE THESIS OF

Michael C. Spillane for the degree of Doctor of Philosophy

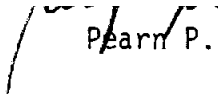
in Oceanography presented on May 20, 1980

Title: A MODEL OF WIND-FORCED VISCOUS CIRCULATION NEAR

COASTAL BOUNDARIES

Redacted for privacy

Abstract approved: \_\_\_\_\_

 P. P. Niiler

A time-dependent model for the response to atmospheric forcing of a homogeneous ocean overlying a continental shelf is considered. The effect of friction is parameterized with surface and bottom Ekman layers of finite thickness. With a Fourier decomposition over frequency and alongshore wavenumber, a second order differential equation for the sea surface profile results. This is solved numerically. In particular, when forcing by the alongshore wind-stress alone is considered, with no across shelf variation in this component, the spectral properties of the model may be described in terms of a set of transfer functions for coastal sealevel and the velocity field.

With an assumed wavenumber dependence for the alongshore wind-stress, computed model predictions of the frequency response of the shelf are formed and compared with the wind-coherent sealevel and horizontal currents on the Oregon shelf. The close agreement found indicates that the subinertial variability of the Oregon coastal zone is dominated by the viscous, barotropic response to alongshore wind-stress forcing.

A Model of Wind-Forced Viscous Circulation  
near Coastal Boundaries

by

Michael Cornelius Spillane

A THESIS

submitted to

Oregon State University

in partial fulfillment of  
the requirements for the  
degree of

Doctor of Philosophy

Completed May 20, 1980

Commencement June 1981

APPROVED: Redacted for privacy

---

Professor of Oceanography  
in charge of major

Redacted for privacy

---

Dean of the School of Oceanography

Redacted for privacy

---

Dean of Graduate School

Date thesis is presented May 20, 1980

Typed by Nancy Kneisel for Michael C. Spillane

## ACKNOWLEDGEMENTS

To my major professor, Dr. P. P. Niiler, for his guidance in the formulation of this project, and his encouragement to see it through. Funding for the study was provided by the National Science Foundation, Grant number OCE 7820766.

My gratitude for their assistance goes to William Gilbert and Henry Pittock, who provided the Oregon data in a convenient form. These data are maintained at Oregon State University under the supervision of Dr. R. L. Smith. The Munk-Cartwright fit was made by Chet Koblinsky, whose assistance in computer related problems was often sought.

To my mother for her long-range support, my friend and fellow student Phyllis Stabeno for her help in the typing of the first draft, and who together with many other friends and acquaintances made my stay at Oregon State a most enjoyable one.

## TABLE OF CONTENTS

I. Introduction	1
II. The Model	5
Fourier Transform Representation	8
The Nearshore Boundary Condition	13
The Offshore Boundary Condition	14
Horizontal Non-divergence and Simplified Forcing	15
The Spectral Transfer Function and the Coherent Coherent Response	16
The Vertical Component of Velocity	21
III. Implementation and Properties of the Model	24
Finite Difference Solution	24
The Regularity Condition at the Coast	25
Model Topography	26
The Transfer Functions	28
Parameter Dependence of the Transfer Functions	35
The Free Wave Solution	42
IV. Data Analysis and Model Intercomparison	49
Data Description	49
Data Analysis	52
Stationarity of the Data	53
The Coherent Response of Sealevel to the Wind	58
The Coherent Response of Horizontal Currents	61

Intercomparison of Model and Experiment	64
Cross-shelf Phase Differences	68
Balances in the Continuity and Horizontal Momentum Equations	72
V. Summary and Conclusions	77
Bibliography	81
Appendix A	85
Appendix B	87

## LIST OF ILLUSTRATIONS

<u>Figure</u>		<u>Page</u>
1	Schematic representation of the shelf model.	6
2	Standard model fit to the Oregon shelf, averaged over the region shown in the inset map.	27
3	The transfer function (real part) for coastal sealevel, with an Ekman depth of ten meters. The inviscid dispersion curves of the first three modes are superimposed.	29
4	The transfer function (imaginary part) for coastal sealevel, with an Ekman depth of ten meters.	30
5	Schematic representation of the response of a damped harmonic oscillator to periodic forcing.	32
6	Transect in wavenumber of the transfer functions of coastal sealevel and the horizontal components of velocity for non-dimensional frequency $\sigma = 0.2$ .	34
7	The influence of the nearshore boundary condition on the integrated transfer function. Curve (a) is for the regularity condition, curves (b), (c) and (d) are for no-flow with wall heights of 12, 24 and 43 meters.	36
8	Alternate model topographic profiles considered for their effect on the integrated transfer function. Also shown are the wall positions of the boundary condition discussion.	38
9	The effect of topographic profile on the integrated transfer function.	40
10	The influence of Ekman layer thickness on the integrated transfer function.	41
11	Dispersion relation for viscous-damped free shelf waves with Ekman depths of one and ten meters.	45

<u>Figure</u>		<u>Page</u>
12	Attenuation characteristics of viscous-damped free shelf waves. Also indicated at discrete points is the ratio of attenuation length to wavelength.	46
13	Location of the current meter moorings used in this study.	51
14	Reduction of the tidal component of sealevel using a Munk-Cartwright fit.	54
15	Time series of alongshore wind stress, adjusted sealevel and current from the Sunflower site for the year 1975.	56
16	Stationarity test for six years of adjusted sealevel at Newport, Oregon. 1973-1978.	57
17	Ensemble averaged autospectra for summer and winter seasons. The 95% confidence ranges are shown in the upper right hand corners.	59
18	The coherent response of adjusted coastal sealevel, 1973-1978 with the estimated 95% confidence range.	62
19	The coherent response of un-corrected coastal sealevel 1969-1978.	63
20	Ensemble averaged autospectra and coherences with the alongshore wind stress for the horizontal components of velocity.	65
21	Model fit to the coherent response of adjusted coastal sealevel.	67
22	Model fit to the coherent response of horizontal currents at mid-depth over the 100 meter isobath. The estimated 90% confidence ranges are indicated. For the onshore component only estimates based on coherences significant at the 90% level are displayed.	69



Figure

Page

- |    |                                                                                                                                                                                                                             |    |
|----|-----------------------------------------------------------------------------------------------------------------------------------------------------------------------------------------------------------------------------|----|
| 23 | Cross-shelf variation in model phase and response amplitude. Curves (a) and (b) are for $\sigma = 0.2$ , curves (c) and (d) for $\sigma = 0.55$ . For (a) and (c) the Ekman depth is ten meters, for (b) and (d) one meter. | 71 |
| 24 | Balances in the continuity equation for Ekman depths of one and ten meters.                                                                                                                                                 | 73 |
| 25 | Balances in the horizontal momentum equations for Ekman depths of one and ten meters.                                                                                                                                       | 75 |

## LIST OF TABLES

<u>Table</u>		<u>Page</u>
1	Summary of Oregon shelf data used in the computation of the wind-coherent response.	50
2	Rotation angles (positive clockwise) of local topographic axes for each current meter mooring, and spatial separations from Newport, Oregon.	60

# A MODEL OF WIND-FORCED VISCOUS CIRCULATION NEAR COASTAL BOUNDARIES

## I. INTRODUCTION

Studies of sealevel and current meter record spectra from continental shelves show the existence of low frequency oscillations with periods ranging from a few days to a few weeks. The fluctuations are in many cases related to local atmospheric variables and, like these fields, are often coherent over alongshore distances of several hundred kilometers. Theoretical models demonstrate the possibility of a variety of forced and wavelike motions of the appropriate scales. Among these are barotropic continental shelf waves, which are topographic Rossby waves, trapped near the coastal boundary through the agency of vorticity. This mechanism is clearly described by Longuet-Higgins (1968a, 1968b), both for the discontinuous depth profiles with which the earlier models were concerned and the later continuous profiles. The models themselves, and the bulk of the observational evidence, are reviewed by LeBlond and Mysak (1977), Mysak (1980) and Allen (1980).

Continental shelf waves can originate or be driven by processes in the ocean interior, as considered for example by Kroll and Niiler (1976) and Allen and Romea (1980). On the other hand the high correlation often observed between currents or sealevel and local

meteorological variables suggests that continental shelf motions may be generated on the shelf by the passage of mesoscale atmospheric disturbances. Early studies considered atmospheric pressure as the driving force but, since these shelf motions involve vorticity, Adams and Buchwald (1969) conclude that the alongshore component of wind stress is a much more effective causal agent. Indeed those models involving pressure forcing often invoked resonance arguments which, because of the large length scales involved and the effects of friction, must be rather unlikely.

The models to date have often been inviscid and cannot account for the observed phase relationships found in shelf measurements. When diffusion is included it is most often parameterized through a bottom friction coefficient, as for example in Mysak (1967) and the diagnostic calculation of Hsueh and Peng (1978). Brink and Allen (1978) have also used this parameterization in showing that the effect of friction on shelf waves is to reduce the phase lag, between the alongshore component of velocity and the forcing, from the value predicted by frictionless models. Their results explain the phase variation observed across continental shelves (Sobey, 1977; Brink, Allen and Smith, 1978), where nearshore fluctuations lead those farther offshore.

Turbulent boundary layers frequently occupy a considerable portion of the water column, especially in shallow regions. This is demonstrated by Smith and Long (1976) for the Washington continental shelf and by Kundu (1977) off Oregon-Washington and northwest

Africa. It thus seems desirable to develop a model of time-dependent forcing on the shelf in which friction can act throughout the water column. It is to this problem that the present study is addressed. Ekman friction with constant vertical eddy diffusivity is used to parameterize the diffusion of vorticity into a homogeneous ocean from the atmosphere, and from the ocean to the bottom. The water depth is allowed to decrease to zero at the coast so that the surface and bottom boundary layers merge.

With zero water depth at the coast the required boundary condition is that all properties of the flow field be regular there. This is in contrast to the nearshore boundary condition most frequently imposed in the literature where no net onshore flow is required at a vertical wall. The results of this study indicate that such a coastal wall may lead to incorrect predictions of coastal sealevel amplitude and currents in the nearshore zone, unless the wall height is less than the boundary layer thickness necessary to account for the effects of vertical eddy diffusion.

The approximate linear equations of motion are Fourier decomposed over frequency and alongshore wavenumber and integrated vertically. The result is a two-point boundary value problem for the transform of adjusted sea surface elevation. The solution of this problem allows a spectral representation of the response of coastal sealevel and the horizontal and vertical components of velocity over the shelf to atmospheric forcing. The spectral representation takes on a particularly convenient form when each component of the forcing

is treated separately and is assumed not to vary across the shelf. The properties of the model may then be discussed, independently of the spectral characteristics of the forcing field, through a set of transfer (or admittance) functions. This study concentrates on the shelf response to alongshore wind stress.

A further objective of the study is to compare the predictions of the model with the observed behaviour of coastal sealevel and horizontal currents over the shelf. Data for these variables and for the forcing do not allow the estimation of joint wavenumber-frequency spectra and as a result the spectral model must be integrated, at least over wavenumber. This is done assuming spatial and temporal stationarity of the wind when its wavenumber and frequency dependencies are separable. With an assumed wavenumber dependence of the wind, based on available information, and an Ekman depth of ten meters the model predictions are found to be in excellent agreement, both in amplitude and phase with observations from the Oregon shelf. Thus the subinertial variability of this region may be largely accounted for with simple linear barotropic dynamics in response to alongshore wind stress.

## II. THE MODEL

Consider a homogeneous ocean of density  $\rho_0$  in a semi-infinite region, illustrated in figure 1. The water is of constant depth except in the vicinity of the boundary. Here the continental shelf and slope are represented by a topographic profile invariant in the alongshore direction. In the fluid adjacent to the boundary the effect of the topography on vorticity is assumed to be of far greater importance than the  $\beta$ -effect so that  $f$ -plane dynamics are used. Cartesian coordinates are drawn with  $x$  offshore,  $y$  alongshore and  $z$  vertically upward. The mean shoreline is at  $x = 0$ , the undisturbed free surface at  $z = 0$  and the bottom at  $z = -H(x)$ .

In the absence of strong mean flows the linearized equations of motion are

$$u_x + v_y + w_z = 0 \quad (1)$$

$$u_t - fv = -g\zeta_x + \kappa u_{zz} \quad (2)$$

$$v_t + fu = -g\zeta_y + \kappa v_{zz} \quad (3)$$

Here subscripts denote partial differentiation,  $(u,v,w)$  are the offshore, alongshore and vertical components of velocity,  $f$  is the constant Coriolis parameter and  $g$  the gravitational acceleration. The effect of diffusion has been parameterized through a constant vertical eddy coefficient  $\kappa$ . The quantity  $\zeta(x,y,t)$  is the adjusted sea level,

$$\zeta = \eta - p_a$$

where  $\eta$  is the actual sea surface elevation and  $p_a$  the negative of atmospheric pressure expressed in units of water height.

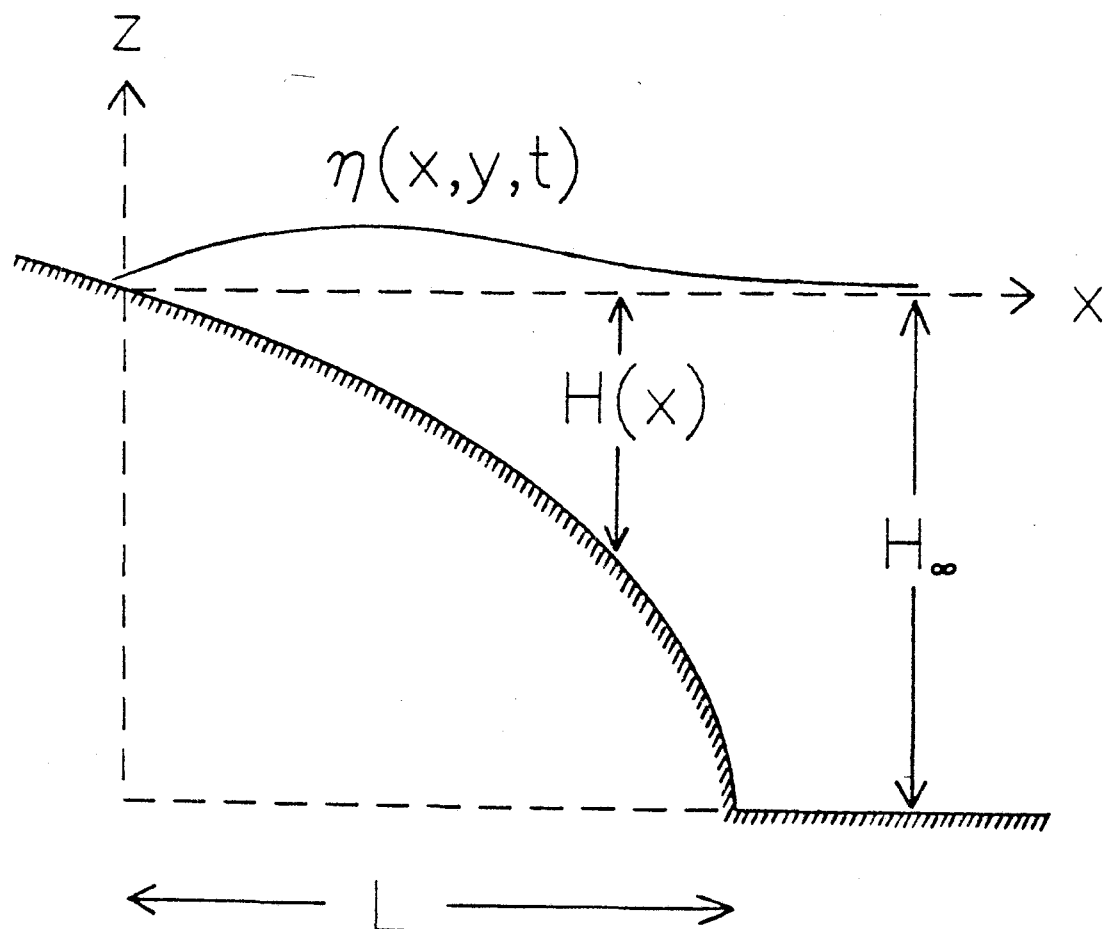


Figure 1. Schematic representation of the shelf model.



We introduce the following scales

$$(x, y, z, t) \rightarrow (L, L, H_0, f^{-1})$$

$$(u, v, w, \zeta) \rightarrow (u_0, u_0, u_0 H_0 / L, u_0 f L / g)$$

where  $L$  is the shelf-slope width,  $H_0$  a depth characteristic of the shelf region and  $u_0$  a characteristic horizontal velocity.

Then in non-dimensional terms, equations (2) and (3) become

$$u_t - v = -\zeta_x + \mu u_{zz} \quad (4)$$

$$v_t + u = -\zeta_y + \mu v_{zz} \quad (5)$$

where the friction parameter  $\mu$  is a vertical Ekman number

$$\mu = \frac{\kappa}{f H_0^2} = (h_E / H_0)^2$$

Here

$$h_E = (\kappa / f)^{1/2}$$

is a depth characteristic of the frictional boundary layers and is henceforth referred to as the Ekman depth.

The boundary conditions employed are

- 1) Horizontal shear stress due to the wind at the surface
- 2) No-slip at the bottom,  $z = -H(x)$ .

If  $\tau_0$  is a scale characteristic of wind stress magnitude then

$$u_0 = \frac{\tau_0}{\rho_0 f H_0}$$

and the non-dimensionalized boundary conditions may be written

$$(\tau^x, \tau^y) = \mu(u_z, v_z) \quad , \text{ at } z = \eta(x, y, t) \quad (6)$$

$$(u, v) = 0 \quad , \text{ at } z = -H(x) \quad (7)$$

The boundary conditions at the shoreline and at the slope-interior junction will be discussed later.

### Fourier Transform Representation

We now Fourier decompose the wind stress, the velocity components and the adjusted sealevel over frequency and alongshore wavenumber.

For a general function the Fourier transform pairing is

$$f(x,y,z,t) \leftrightarrow F(x,\lambda,z,\sigma)$$

where

$$f(x,y,z,t) = (2\pi)^{-2} \int_{-\infty}^{\infty} \int_{-\infty}^{\infty} F(x,\lambda,z,\sigma) e^{i(\lambda y + \sigma t)} d\lambda d\sigma$$

and

$$F(x,\lambda,z,\sigma) = \int_{-\infty}^{\infty} \int_{-\infty}^{\infty} f(x,y,z,t) e^{-i(\lambda y + \sigma t)} dy dt$$

Here  $\sigma$  and  $\lambda$  are the frequency ( $\omega$ ), and the alongshore wavenumber ( $\ell$ ) nondimensionalized with the inertial frequency and the shelf-slope width respectively

$$\sigma = \omega / f \quad , \quad \lambda = \ell L$$

It should be noted that when Fourier transformation is employed in purely inviscid problems of continental shelf circulation, inversion may lead to ambiguous results due to the presence of poles on the real axis. However, as demonstrated by Adams and Buchwald (1969), such ambiguity does not arise when frictional damping is present. In effect the presence of damping imposes a radiation condition at infinity in the alongshore direction that confines our attention to outgoing waves.

Using upper case letters to denote Fourier transforms we write

$$(\tau^x, \tau^y) \leftrightarrow (T^x, T^y)$$

$$(u, v, w) \leftrightarrow (U, V, W)$$

$$\zeta, p_a \leftrightarrow Z, P_a$$

Note that  $(\tau^x, \tau^y)$ , and  $p_a$  have no  $z$ -dependence, and so neither will

their transforms.

Equations (4) and (5) now become

$$i\sigma U - V = -Z_x + \mu U_{ZZ}$$

$$i\sigma V + U = -i\lambda Z + \mu V_{ZZ}$$

These have a depth independent particular solution for U and V in terms of Z

$$(1-\sigma^2)U = -i\sigma(Z_x + \frac{\lambda}{\sigma}Z)$$

$$(1-\sigma^2)V = Z_x + \lambda\sigma Z$$

The homogenous equations for both U and V take the form

$$\left\{ \frac{\partial^4}{\partial z^4} - \frac{2i\sigma}{\mu} \frac{\partial^2}{\partial z^2} + \frac{1-\sigma^2}{\mu^2} \right\} U = 0$$

which on assuming a solution of the form  $\exp(\alpha z)$  leads to the roots  $\pm\alpha$ ,  $\pm\beta$  where

$$\beta = \left(\frac{1+\sigma}{2\mu}\right)^{\frac{1}{2}} (1+i)$$

$$\alpha = \left(\frac{1-\sigma}{2\mu}\right)^{\frac{1}{2}} (1-i)$$

The depth dependent part of the velocity components can be conveniently expressed in terms of the functions

$$\phi_\beta = \frac{\sinh\beta(z+H)}{\beta \cosh\beta H} \qquad \phi_\alpha = \frac{\sinh\alpha(z+H)}{\alpha \cosh\alpha H}$$

$$\psi_\beta = \frac{\cosh\beta z}{\cosh\beta H} \qquad \psi_\alpha = \frac{\cosh\alpha z}{\cosh\alpha H}$$

as

$$U = A\phi_\beta + B\phi_\alpha + C\psi_\beta + D\psi_\alpha$$

$$V = -i(A\phi_\beta - B\phi_\alpha + C\psi_\beta - D\psi_\alpha)$$

The boundary conditions (6),(7) allow the coefficients A,B,C,D to

be determined. When (6) is imposed at the undisturbed free surface  $z = 0$  we obtain

$$\begin{aligned} A &= (T^X + iT^Y)/2\mu \\ B &= (T^X - iT^Y)/2\mu \\ C &= -i(Z_X - \lambda Z)/(1+\sigma) \\ D &= i(Z_X + \lambda Z)/(1-\sigma) \end{aligned}$$

so that

$$U = \left(\frac{\phi_\beta + \phi_\alpha}{2\mu}\right)T^X + i\left(\frac{\phi_\beta - \phi_\alpha}{2\mu}\right)T^Y - \frac{i\sigma}{1-\sigma^2} \left\{ \left(1 + \frac{1-\sigma}{2}\psi_\beta - \frac{1+\sigma}{2}\psi_\alpha\right)Z_X + \frac{\lambda}{\sigma} \left(1 - \frac{1-\sigma}{2}\psi_\beta - \frac{1+\sigma}{2}\psi_\alpha\right)Z \right\} \quad (8)$$

$$V = -i\left(\frac{\phi_\beta - \phi_\alpha}{2\mu}\right)T^X + \left(\frac{\phi_\beta + \phi_\alpha}{2\mu}\right)T^Y + \frac{1}{1-\sigma^2} \left\{ \left(1 - \frac{1-\sigma}{2}\psi_\beta - \frac{1+\sigma}{2}\psi_\alpha\right)Z_X + \lambda\sigma \left(1 + \frac{1-\sigma}{2}\psi_\beta - \frac{1+\sigma}{2}\psi_\alpha\right)Z \right\} \quad (9)$$

Note that the roots  $\beta$  and  $\alpha$  and their associated  $\phi$  and  $\psi$  functions correspond to clockwise and counterclockwise components respectively of the motion. This may be seen by forming the complex velocities  $U + iV$  and  $U - iV$ .

We now integrate vertically the continuity equation (1). This leads to

$$\frac{\partial}{\partial x} \int_{-H}^n u \, dz + \frac{\partial}{\partial y} \int_{-H}^n v \, dz + \epsilon n_t = 0$$

where  $\epsilon$  is a dimensionless parameter that expresses the relative importance of surface divergence.

$$\epsilon = \frac{f^2 L^2}{gH_0} = (L/r_e)^2$$

Here  $r_e$  is the external Rossby radius of deformation which for scale

values typical of continental shelves is considerably greater than the shelf width  $L$ .

In applying the integrated continuity equation to the model we replace the upper limit of integration by zero in order that the model remain linear. Then in Fourier space we have

$$\frac{\partial}{\partial x} \int_{-H}^0 U dz + \frac{\partial}{\partial y} \int_{-H}^0 V dz + i\sigma\epsilon(Z + P_a) = 0 \quad (10)$$

The depth dependence of  $U$  and  $V$  is confined to the  $\phi$  and  $\psi$  functions and we define

$$\phi_\beta = \int_{-H}^0 \phi_\beta dz = (1 - \text{sech}^2 \beta H) / \beta^2$$

$$\psi_\beta = \int_{-H}^0 \psi_\beta dz = (\tanh \beta H) / \beta$$

with analogous expressions for  $\phi_\alpha$  and  $\psi_\alpha$ . Then substitution of expressions (8) and (9) for  $U$  and  $V$  into (10) leads to

$$\begin{aligned} (hZ_x)_x + \left\{ \frac{\lambda H_x}{\sigma} - \lambda^2 h - \epsilon(1 - \sigma^2) \right\} Z \\ = \frac{1 - \sigma^2}{2\mu\sigma} \left\{ (\phi_\beta - \phi_\alpha)(T_x^y - T_y^x) - i(\phi_\beta + \phi_\alpha)(T_x^x + T_y^y) \right. \\ \left. - i(\phi_\beta + \phi_\alpha)_x T_x^x + (\phi_\beta - \phi_\alpha)_x T_x^y \right\} + \epsilon(1 - \sigma^2) P_a \end{aligned} \quad (11)$$

where

$$h = H + \frac{1 - \sigma}{2\sigma} \psi_\beta - \frac{1 + \sigma}{2\sigma} \psi_\alpha$$

$$H = H - \frac{1 - \sigma}{2} \psi_\beta - \frac{1 + \sigma}{2} \psi_\alpha$$

The forcing terms on the right hand side of (11) are associated respectively with the effects of

- 1) Wind stress curl
- 2) Wind stress divergence
- 3) Offshore wind stress acting on the topographic slope
- 4) Alongshore wind stress acting on the topographic slope
- 5) Atmospheric pressure

Equation (11), when combined with suitable boundary conditions at the shoreline and at the slope-interior junction, describes the viscous response of adjusted sea surface elevation to forcing at wavenumber-frequency  $(\lambda, \sigma)$ . The associated horizontal circulation can be obtained from equations (8) and (9) and the vertical component of velocity derived as discussed later.

The homogeneous version of equation (11) is reminiscent of the inviscid theory, for example equation (15) of Mysak (1979). In our notation

$$(HZ_x)_x + \{\lambda H_x / \sigma - \lambda^2 H - \epsilon(1-\sigma^2)\} Z = 0$$

However instead of  $H$ , equation (11) contains the frequency dependent functions  $h$  and  $H$  which might be described as "equivalent depths" for the viscous problem. In fact in the limit as  $\mu \rightarrow 0$ , when diffusion is confined to infinitely thin boundary layers, equation (11) reduces to

$$(HZ_x)_x + \{\lambda H_x / \sigma - \lambda^2 H - \epsilon(1-\sigma^2)\} Z = -\frac{i}{\sigma}(T_x^y - T_y^x) + (T_x^x + T_y^y) + \epsilon(1-\sigma^2)P_a$$

which is in exact agreement with the inviscid theory.

The Nearshore Boundary Condition

Two cases arise, depending on whether the undisturbed water depth tends to zero at the coast, or to some finite non-zero value. The latter situation of a vertical wall, though seemingly unrealistic, except perhaps for motions with very large scales, occurs frequently in the literature. This is particularly true in the case of inviscid models where the rationale appears to be that one thereby excludes an inner region where diffusive effects are to be expected.

In the case of non-zero water depth at the coast the appropriate boundary condition is that of no net onshore flow. Vertical integration of equation (8) at  $x = 0$  leads to the condition

$$hZ_x + \frac{\lambda H}{\sigma} Z = \frac{1-\sigma^2}{2\mu\sigma} \{(\phi_\beta - \phi_\alpha)T^y - i(\phi_\beta + \phi_\alpha)T^x\} \quad (12)$$

In our model horizontal eddy diffusivity has been ignored. This is valid over shelves of gentle slope (Allen, 1980), but is inappropriate in the vicinity of a discontinuity of depth, where horizontal eddy diffusion leads to a variety of boundary layers. We will therefore implement our model for topographic profiles with zero depth at  $x = 0$ . In this case equation (11) has a singularity at the origin. In order that  $Z$  and the velocity components be well behaved we seek regular solutions only. The condition for regular behaviour is that

$$|Z_x(x=0)| < M, \text{ a constant.} \quad (12a)$$

Regular solutions allow a net onshore flow at the coast. This represents the possible run-up on the sloping beach. We will see however that our viscous model is insensitive to the choice of nearshore boundary condition provided the wall height is less than the Ekman depth.

### The Offshore Boundary Condition

The ocean interior is modelled as being of uniform depth. Then equation (11) reduces to

$$hZ_{xx} - \{\lambda^2 h + \epsilon(1-\sigma^2)\}Z = \frac{1-\sigma^2}{2\mu\sigma} \{(\phi_\beta - \phi_\alpha)(T_x^y - T_y^x) - i(\phi_\beta + \phi_\alpha)(T_x^x + T_y^y)\} + \epsilon(1-\sigma^2)P_a \quad (13)$$

where  $h, H$  and the  $\phi$  functions are now independent of  $x$ . Solutions to (11) and (13) are to be matched at the slope-interior junction  $x = 1$ . This matching will in general force a shelf response due to the circulation of the ocean interior. Our interest lies mainly in the shelf response rather than in shelf-interior interactions so we confine ourselves to solutions of (13) that decay with increasing  $x$ . In the next section we introduce some simplifying assumptions on the model that facilitate the identification of such coastal-trapped solutions as well as allowing a simple spectral representation of shelf response to forcing by the alongshore component of windstress.



### Horizontal Non-Divergence and Simplified Forcing

In equations (11) and (13) the term  $\varepsilon(1-\sigma^2)Z$  represents the effect of surface divergence. This may be important in laboratory situations and the term is retained for example by Caldwell, Cutchin and Longuet-Higgins (1972). We choose to eliminate it, thus restricting ourselves to horizontally non-divergent motions. Surface divergence might be expected to play some part in the shallow regions nearshore. However, effects of comparable importance may already have been excluded in our integration of the continuity equation, where the upper limit of integration was replaced by zero in the interests of linearization. The non-linear problem of finite amplitude gravity waves on a sloping beach has been treated by Carrier and Greenspan (1958). Such problems may be solved by characteristics but our viscous model without the long wave approximation does not lend itself to such treatment.

The term  $\varepsilon(1-\sigma^2)P_a$  in equations (11) and (13) represents the effect of atmospheric pressure in the generation of non-isostatic sealevel fluctuations. In our linear model the effect may be separated from the forced response due to wind stress. The latter is believed to be the more important. We further restrict our attention to forcing due to alongshore wind stress, and ignore any variation of this component across the shelf.

$$(\tau^x, \tau^y) = (0, \tau^y(y,t))$$

This eliminates forcing due to the wind stress curl and equation (13) becomes, subject to the above restrictions

$$Z_{xx} - \lambda^2 Z = \lambda \frac{1-\sigma^2}{2\mu\sigma} \left( \frac{\phi_\beta + \phi_\alpha}{h} \right)_\infty T^y$$

where the subscript  $\infty$  denotes the value in the constant depth interior. The particular solution to this is

$$Z = - \frac{1-\sigma^2}{2\mu\sigma\lambda} \left( \frac{\phi_\beta + \phi_\alpha}{h} \right)_\infty T^y$$

due to wind stress divergence in the open ocean. The homogeneous equation has a solution

$$Z \propto \exp(-|\lambda|x)$$

where the decaying form has been chosen to represent coastal trapping in the semi-infinite region  $x \geq 0$ . The deep water boundary condition at  $x = 1$  can now be written as

$$Z_x + |\lambda|Z = - \operatorname{sgn}\lambda \frac{1-\sigma^2}{2\mu\sigma} \left( \frac{\phi_\beta + \phi_\alpha}{h} \right)_\infty T^y$$

where

$$\operatorname{sgn}\lambda = \lambda/|\lambda|$$

### The Spectral Transfer Function and the Coherent Response

Assuming horizontal non-divergence and the simplified forcing described above, the transform of adjusted sealevel must satisfy

$$(hZ_x)_x + \{\lambda H_x/\sigma - \lambda^2 h\}Z = \frac{1-\sigma^2}{2\mu\sigma} \{(\phi_\beta - \phi_\alpha)_x + \lambda(\phi_\beta + \phi_\alpha)\} T^y \quad (14)$$

with

$$hZ_x + \frac{\lambda H_x}{\sigma} Z = \frac{1-\sigma^2}{2\mu\sigma} (\phi_\beta - \phi_\alpha) T^y, \quad x = 0 \quad (15)$$

or

$$Z_x(x=0) < M, \quad \text{a constant} \quad (15a)$$

and

$$Z_x + |\lambda|Z = - \operatorname{sgn}\lambda \frac{1-\sigma^2}{2\mu\sigma} \left( \frac{\phi + \bar{\phi}}{h} \right)_{\infty} T^y, \quad x = 1 \quad (16)$$

These equations are linear in  $T^y(\lambda, \sigma)$ . If  $T^y$  is replaced by unity the solution of these equation results in what might be termed the Spectral Transfer Functions for sea surface elevation and the various properties of the flow field derivable from it. If the transfer function of any one of these variable is denoted by  $R(x, \lambda, z, \sigma)$  then the overall response of that variable to the actual forcing is found by superimposing the wavenumber-frequency spectral decomposition of the alongshore wind stress field.

$$F(x, \lambda, z, \sigma) = R(x, \lambda, z, \sigma) T^y(\lambda, \sigma) \quad (17)$$

The various spectral transfer functions thus embody the properties of our simplified viscous forced model. In the next chapter these functions are computed and examined in the light of their dependence on the choice of vertical Ekman number, topographic profile and the boundary condition imposed at the coast.

It should be noted that a similar set of transfer functions could be derived for forcing due to either atmospheric pressure or the onshore component of wind stress if these are assumed not to vary across the shelf. The overall response would then be given by a linear superposition of these effects. The wind stress curl does not lend itself to this simple treatment insofar as it contains the term  $T_x^y$ .

A further objective of this study is to compare model predictions with actual field observations derived from tide gage and current meter records. These data from fixed locations may be

represented either in the time or the frequency domain. Wavenumber information is rarely available so that equation (17) must be inverted at least over wavenumber. This requires the knowledge of the joint wavenumber-frequency transform of alongshore windstress. Weather stations on the U.S. Pacific coast are typically separated by several hundred kilometers, except during brief intensive studies, and are strongly influenced by orographical effects (Halpern, 1974). Syntheses of the wind field from atmospheric pressure data, such as used in producing an Upwelling Index (Bakun, 1973) are also limited in spatial resolution.

The application of standard spectral techniques to the available data allows the identification of the wind coherent part of each observed property of the coastal flow regime. For each such property  $F$  we define a Coherent Response,  $R_c$  and phase  $\theta_c$

$$R_c(\omega) = \frac{\gamma^2 S_F}{S_T} \quad (18)$$

$$\theta_c(\omega) = \arg(S_{FT}) \quad (18a)$$

Here  $S_F$ ,  $S_T$  denote the frequency autospectra of  $F$  and the alongshore wind stress respectively;  $S_{FT}$  is their cross-spectrum and  $\gamma^2$  their squared coherence

$$\gamma^2(\omega) = \frac{|S_{FT}|^2}{S_F S_T} \quad (19)$$

Inversion of equation (17) leads to

$$f(x,y,z,t) = \int_{-\infty}^{\infty} \int_{-\infty}^{\infty} R(x,\delta,z,\xi) \tau^y(y-\delta,t-\xi) d\delta d\xi \quad (20)$$

Here  $R(x, \lambda, z, \sigma)$ , the inverse transform of the Transfer function, is the system function of a single input linear system relating  $f$  to  $\tau^y$ . The application of some further concepts of linear systems analysis allows the definition of a Model Response,  $R_M$  and phase  $\theta_M$  which, subject to some assumptions on the wind field, may be compared with the quantities defined in (18), (18a).

Suppose  $\tau^y(y, t)$  is a stochastic random variable, stationary both in space and time. The system function  $R$  in equation (20) is deterministic but the system output  $f(x, y, z, t)$  will also be a random variable. Auto- and cross-correlation functions for  $\tau^y$  and  $f$  may be defined, which form Fourier transform pairs with the wavenumber-frequency auto- and cross-spectra,

$$S_F(\lambda, \sigma) \leftrightarrow \langle f(x, \delta, z, \xi) f^*(x, y + \delta, z, t + \xi) \rangle$$

$$S_T(\lambda, \sigma) \leftrightarrow \langle \tau^y(\delta, \xi) \tau^*(y + \delta, t + \xi) \rangle$$

$$S_{FT}(\lambda, \sigma) \leftrightarrow \langle f(x, \delta, z, \xi) \tau^*(x, y + \delta, z, t + \xi) \rangle$$

Here  $\langle \dots \rangle$  denotes averaging in both space and time and  $(\dots)^*$  denotes complex conjugation. Explicit reference to the  $x$  and  $z$  dependence of  $S_F$  and  $S_{FT}$  has been suppressed for convenience. The generalization of the systems treatment (for example Bendat and Piersol (1971)) applied to equation (20) leads to

$$S_F(\lambda, \sigma) = |R(x, \lambda, z, \sigma)|^2 S_T(\lambda, \sigma)$$

$$S_{FT}(\lambda, \sigma) = R(x, \lambda, z, \sigma) S_T(\lambda, \sigma)$$

At each point in wavenumber-frequency space the squared coherence, defined in analogy with (19) is unity. The interaction

of a range of wavenumber components may lead to decoherence when frequency spectra are computed.

If  $S_T(\lambda, \sigma)$  is known, or in practice modelled with some algebraic representation, the model response and phase are formed by integration over wavenumber

$$R_M(\sigma) = \frac{\gamma^2 S_F(\sigma)}{S_T(\sigma)} \quad (21)$$

$$\theta_M(\sigma) = \arg(S_{FT}(\sigma)) \quad (21a)$$

with

$$S_F(\sigma) = \int_{-\infty}^{\infty} |R(x, \lambda, z, \sigma)|^2 S_T(\lambda, \sigma) d\lambda$$

$$S_T(\sigma) = \int_{-\infty}^{\infty} S_T(\lambda, \sigma) d\lambda$$

$$S_{FT}(\sigma) = \int_{-\infty}^{\infty} R(x, \lambda, z, \sigma) S_T(\lambda, \sigma) d\lambda$$

and

$$\gamma^2(\sigma) = \frac{S_{FT}(\sigma)}{S_F(\sigma) S_T(\sigma)} \quad (22)$$

The model response  $R_M$  (expressed in dimensional units) and phase  $\theta_M$  may be compared with the coherent response  $R_C$  and phase  $\theta_C$  derived from data. This comparison is attempted in Chapter IV. There it is further assumed that the spectral density  $S_T(\lambda, \sigma)$  may be decomposed as

$$S_T(\lambda, \sigma) = S_1(\lambda) S_2(\sigma) \quad (23)$$

In this case the model response is given by

$$R_M(\sigma) = \left| \int_{-\infty}^{\infty} R(x, \lambda, z, \sigma) S_1(\lambda) d\lambda \right|^2 \quad (24)$$

when  $S_1(\lambda)$ , the assumed wavenumber dependence of the wind, has

been normalized

$$\int_{-\infty}^{\infty} S_1(\lambda) d\lambda = 1$$

The decomposition (23) may be justified in a number of ways. It would result for example if the weather systems causing the wind stress propagate at right angles to the coastline. This was assumed by Brooks (1978) in a study of the coastal response off North Carolina. If on the other hand there is no preferred propagational characteristics for weather systems, so that variations in  $t$  and  $y$  are uncorrelated, this decomposition might also be expected. Variability of the latter type was inferred by Mysak (1967) for the low frequency behaviour of atmospheric pressure fluctuations off Australia. More recently Willebrand (1978) demonstrates that, in the open ocean at mid-latitudes, atmospheric energy is essentially isotropic in north-south wavenumber at subinertial frequencies, even for scales of several thousand kilometers. This lends further support to the decomposition.

#### The Vertical Component of Velocity

The model also allows the vertical component of velocity to be determined. Here we consider only the case of horizontally non-divergent motions with the simplified forcing. If the vertical integration of the continuity equation, rather than extending from  $z = -H(x)$  to the surface, is terminated at some intermediate depth  $z_0 < 0$  then

$$W(z_0) = \frac{i\sigma}{1-\sigma^2} \{ (h(z_0)Z_x)_x + (\frac{\lambda}{\sigma}H(z_0) - \lambda^2h(z_0))Z \} \\ - \frac{iT^y}{2\mu} \{ (\phi_\beta(z_0) - \phi_\alpha(z_0))_x + \lambda(\phi_\beta(z_0) + \phi_\alpha(z_0)) \} \quad (25)$$

Here

$$h(z_0) = (H+z_0) + \frac{1-\sigma}{2\sigma}\psi_\beta(z_0) - \frac{1+\sigma}{2\sigma}\psi_\alpha(z_0)$$

$$H(z_0) = (H+z_0) - \frac{1-\sigma}{2}\psi_\beta(z_0) - \frac{1+\sigma}{2}\psi_\alpha(z_0)$$

$$\psi_\beta(z_0) = (\sinh\beta z_0 + \sinh\beta H)/\beta \cosh\beta H$$

$$\phi_\beta(z_0) = (\cosh\beta(z_0+H) - 1)/\beta^2 \cosh\beta H$$

are generalizations of the earlier functions which were evaluated at the mean free surface  $z = 0$ . The functions  $\psi_\alpha(z_0)$  and  $\phi_\alpha(z_0)$  are defined in an analogous fashion.

Equation (25) allows the vertical component of velocity to be determined at any point in the water column whenever  $Z$  is known. A transfer function for  $W$  can be formed and used to represent the spectral characteristics of the vertical component of velocity.

If in particular  $z_0$  is chosen in the inviscid interior, and the Ekman layers are thin in comparison to the local water depth, equation (25) may be considerably simplified

$$W(z_0) \approx \frac{\sigma}{1-\sigma^2} \{ iz_0 (Z_{xx} - \lambda^2 Z) - \lambda T^y \}$$

Further for this situation

$$Z_{xx} - \lambda^2 Z \approx -\frac{H}{H} Z_x + \frac{\lambda}{\sigma} Z + \frac{i\lambda}{H} T^y$$

and

$$U(z_0 \gg h_E) = \frac{-i\sigma}{1-\sigma^2} (Z_x + \frac{\lambda}{\sigma} Z)$$



so that

$$W(z_0) = \frac{z_0 H}{H} U(z_0) - \left(\frac{H+z_0}{H}\right) \frac{\lambda \sigma}{1-\sigma^2} T^y \quad (26)$$

The transfer functions of  $W$  and  $U$  are thus linearly related at points in the inviscid interior.

If now a model response is formed as in equation (24) and the decomposed wind stress spectrum is taken to be even in  $\lambda$ , the second term on the right of (26) integrates to zero. Then the model responses of  $W$  and  $U$  are identical except for a factor dependent only on the local water depth, the bottom slope and the location chosen within the inviscid interior.

To the extent that these assumptions are valid this relationship between the response of  $U$  and  $W$  can be used to estimate the frequency spectrum of the vertical component of velocity at a position where the onshore velocity spectrum is known.

### III. IMPLEMENTATION AND PROPERTIES OF THE MODEL

#### Finite Difference Solution

Our task is the integration of the two-point boundary value problem defined by equations (14), (15) or (15a) and (16). The inviscid case  $\mu = 0$  has analytic solutions for certain specific topographic profiles, such as the exponential shelf treated by Adams and Buchwald (1969). Indeed some general conclusions may be drawn for classes of profile types in the inviscid case as shown by Huthnance (1975) and Odulo (1975).

The viscous model derived here, with  $\mu \neq 0$  does not allow such analytic treatment. Instead we resort to numerical means. A particularly convenient method for our purposes is described by Lindzen and Kuo (1969). Its implementation results in a complex valued sea surface profile in response to forcing by unit alongshore windstress, subject to the frictional effects imposed by the particular choice of the Ekman number  $\mu$ . From this profile we may obtain the transfer functions for coastal sealevel and selected properties of the velocity field over the shelf, at the wavenumber frequency combination  $(\lambda, \sigma)$ . The process is repeated at a sufficient number of points to give an adequate representation over the  $\lambda$ - $\sigma$  plane.

In this study transfer functions were produced for coastal sealevel and the velocity field  $(U, V, W, U_x, V_y)$  for mid-depths at the 50, 100 and 200 meter isobaths, with values of  $\mu$  equivalent to Ekman depths of one and ten meters. The topographic profile chosen

is representative of the Oregon shelf and is discussed below.

### The Regularity Condition at the Coast

To allow friction to take its full effect in the nearshore region we employ the regularity condition (15a). In order to implement this numerically the various functions in (14) are expanded as power series in  $x$ . The particular and homogeneous solutions are written as regular series expressions

$$\begin{aligned} Z_p &= a_1x + a_2x^2 + \dots \\ Z_H &= 1 + b_1x + b_2x^2 \dots \end{aligned}$$

Collecting like powers of  $x$  in (14) allows the determination of the coefficients  $a_i$ ,  $b_i$ , for a sufficient number of terms to achieve convergence. Matching the regular solution

$$Z = Z_p + CZ_H$$

to the general shelf solution for both  $Z$  and  $Z_x$  at some nearshore point  $x_1 \ll 1$  and eliminating the constant  $C$  results in a boundary condition of the form

$$Z_x + AZ = B \quad , \text{ at } x = x_1$$

where

$$A = -(Z_{Hx}/Z_H) \quad , \text{ at } x = x_1$$

$$B = (Z_{px} + AZ_p) \quad , \text{ at } x = x_1$$

Series expansion for the functions  $h$ ,  $H$  and  $\phi$  are developed in Appendix A, as are the recurrence relations for  $a_i$ ,  $b_i$  that result, for the particular case of topography linear in the nearshore region. In principle recurrence relations could be derived for any nearshore topography though the complexity of the algebra would be greatly increased. Since the linear region need only extend to the position  $x_1 \ll 1$  at which the boundary condition is imposed no great loss of generality results from its use.

#### Model Topography

For a finite difference solution the topography need only be specified at the grid points. Hence we may use either an algebraic representation of the profile, or the actual measured depths. The former may in fact be more reasonable, since the coastal ocean will "feel" an average profile over an alongshore scale related to that of the forcing rather than the irregularities of some particular transect.

A reasonable fit to the Oregon shelf is given by

$$H(x) = \begin{cases} mx & , 0 < x < (2b)^{-1} \\ e^{2bx} & , (2b)^{-1} < x < 1 \\ e^{2b} & , x > 1 \end{cases}$$

with

$$m = 2b \exp(1)$$

The ocean interior has constant depth, while the junction between the linear and exponential sections at  $x = (2b)^{-1}$  is achieved without discontinuity in depth or of slope. A value of  $b = 1.865$  is found

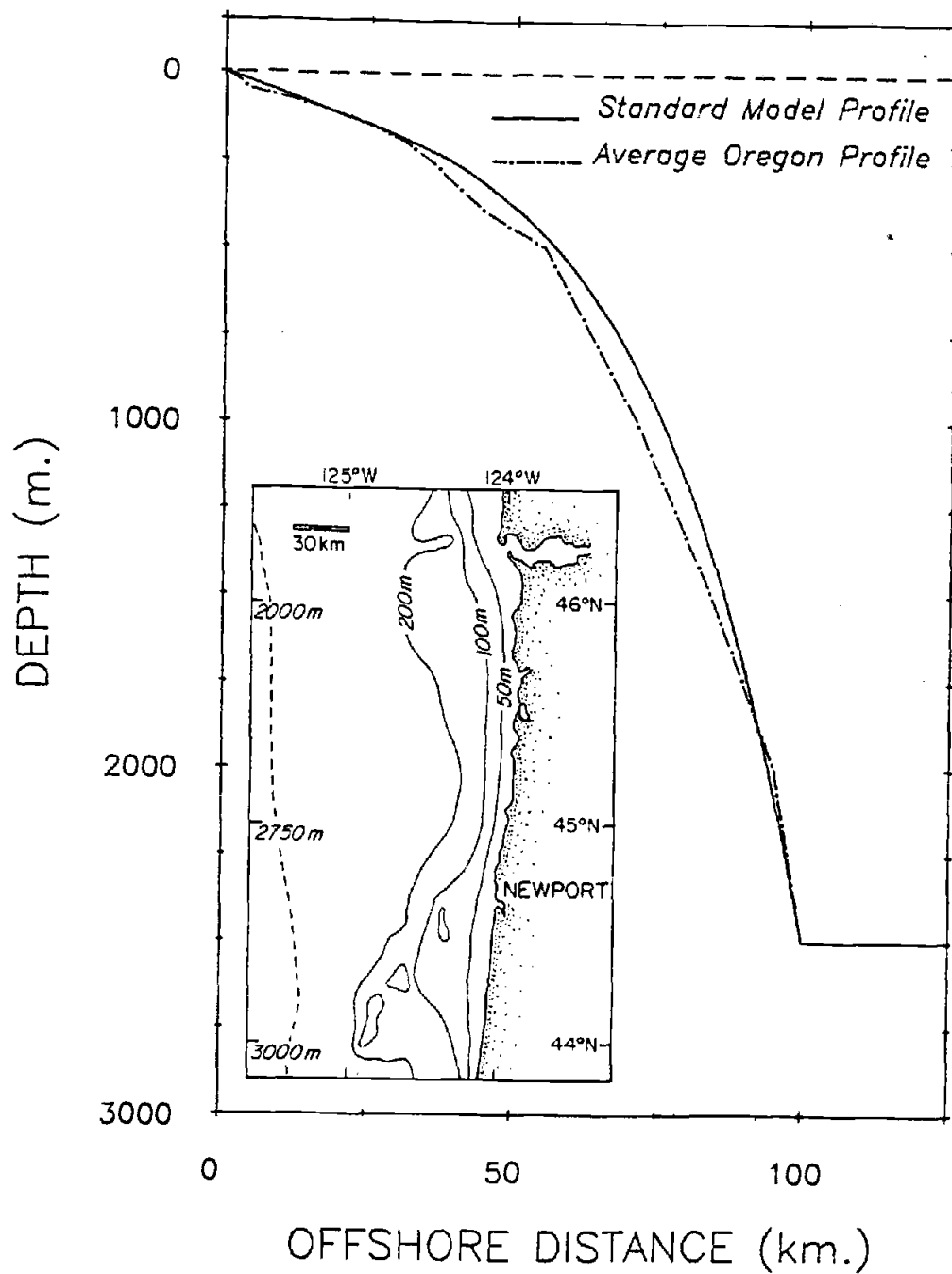


Figure 2. Standard model fit to the Oregon shelf, averaged over the region shown in the inset map.

to best represent the average Oregon profile as illustrated in Figure 2. The Oregon average was computed as the mean of transects at 15' intervals in the range  $44^{\circ}$  to  $46^{\circ}$ N. The dashed line offshore represents the approximate location of the slope-interior junction. The interior depth decreases somewhat from south to north and a mean value of 2500 meters is chosen.

The corresponding dimensional values used are

$$\begin{aligned} L &= \text{Shelf-slope width} &= 100 \text{ km} \\ L/2b &= \text{Width of linear section} &= 26.8 \text{ km} \\ H_0 &= \text{Depth scale of shelf} &= 60 \text{ m} \\ H_{\infty} &= \text{Depth of ocean interior} &= 2500 \text{ m} \end{aligned}$$

Here  $H_0$  is the depth at which the exponential profile, if produced shoreward, would have intersected the coast. This definition is used to facilitate comparison with the simple exponential topography that is frequently employed in the literature.

In the subsequent discussion the topographic profile defined above will be referred to as "Standard".

### The Transfer Functions

In Figures 3 and 4 are displayed the real and imaginary parts of the transfer function for coastal sealevel, based on an Ekman depth of 10 meters. The contours show that sealevel fluctuations are efficiently generated in the vicinity of the dashed lines. These are the dispersion curves for the first three inviscid shelf wave modes for the Standard topography. For our choice of coordinate system the sense of propagation of such waves is consistent with an

Sealevel Transfer Function Real Part Ekman Depth 10m.

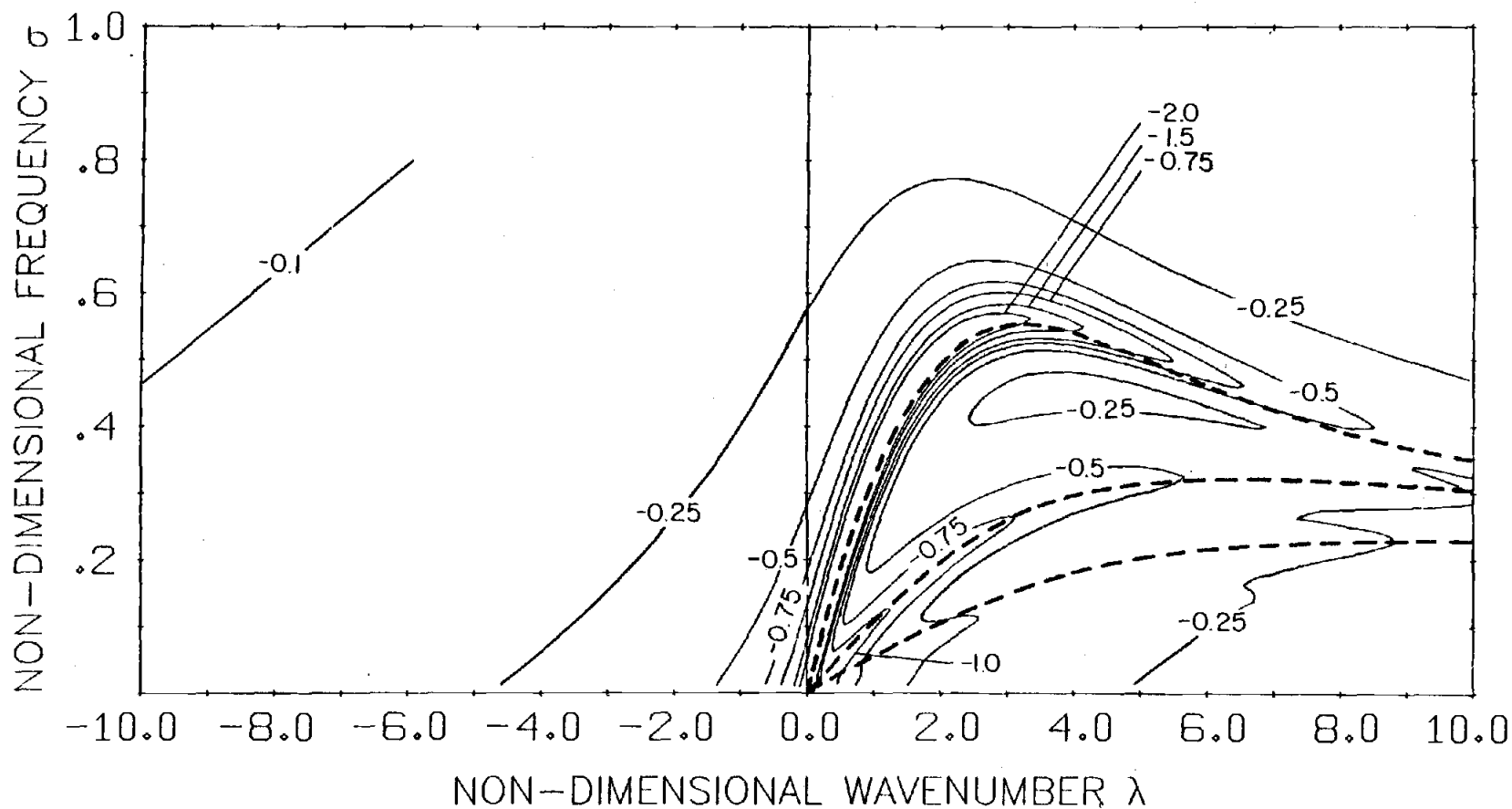


Figure 3. The transfer function (real part) for coastal sealevel, with an Ekman depth of ten meters. The inviscid dispersion curves of the first three modes are superimposed.

Sealevel Transfer Function Imag. Part Ekman Depth 10m.

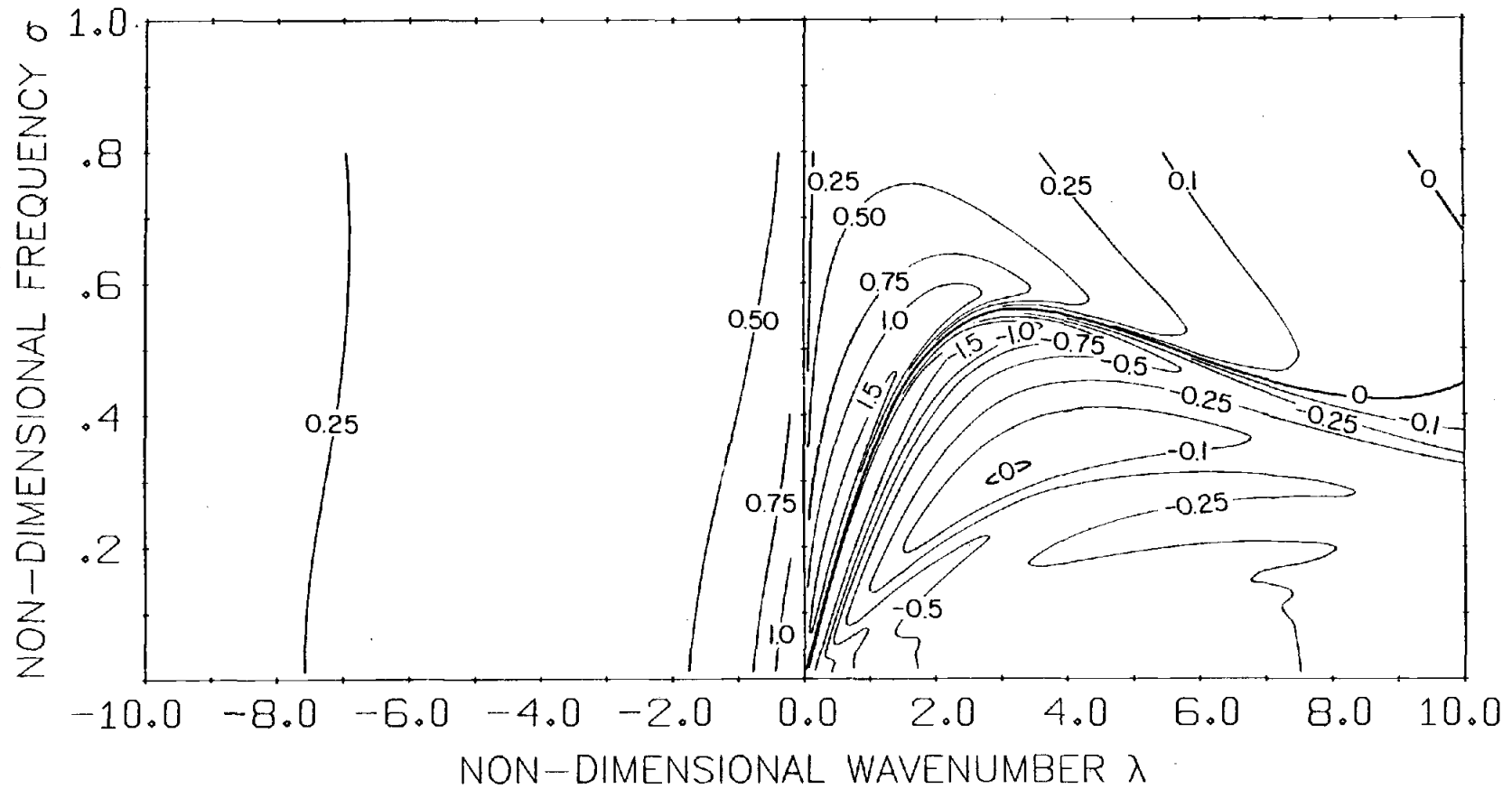


Figure 4. The transfer function (imaginary part) for coastal sealevel, with an Ekman depth of ten meters.



ocean in the Northern hemisphere when wavenumber and frequency are positive. As is normal for shelf profiles of this general shape each inviscid mode has a high frequency cutoff at which the group velocity vanishes. In the next section we will examine briefly the dispersion and attenuation properties of free shelf waves using our viscous model.

Holding wavenumber constant, a transect in frequency through a mode is reminiscent of the response of a damped harmonic oscillator, of natural frequency  $\omega_0$ , to forcing  $\exp(i\omega t)$ . The latter is illustrated schematically in Figure 5. For a damped harmonic oscillator the real part of the response is a modification of the discontinuous undamped situation. In passing through resonance the phase reverses sign. This behavior is observed in our model transfer function. However since the inviscid response of sealevel is in quadrature with the forcing, real and imaginary parts must be interchanged in drawing the analogy with the damped harmonic oscillator.

In Figures 3 and 4 the efficiency of energy transfer from the wind to sealevel fluctuations is seen to decrease in progressing toward higher wavenumbers along each mode. It is greatest for the first mode. It should also be noted that the width in wavenumber of the response ridge broadens as the high frequency cut-off is approached. This effect will be of importance whenever the forcing is broadband in wavenumber. The increased width of the ridge may more than compensate for the decreased amplitude whenever we invert (i.e. integrate) over wavenumber. For such broadband forcing the frequency

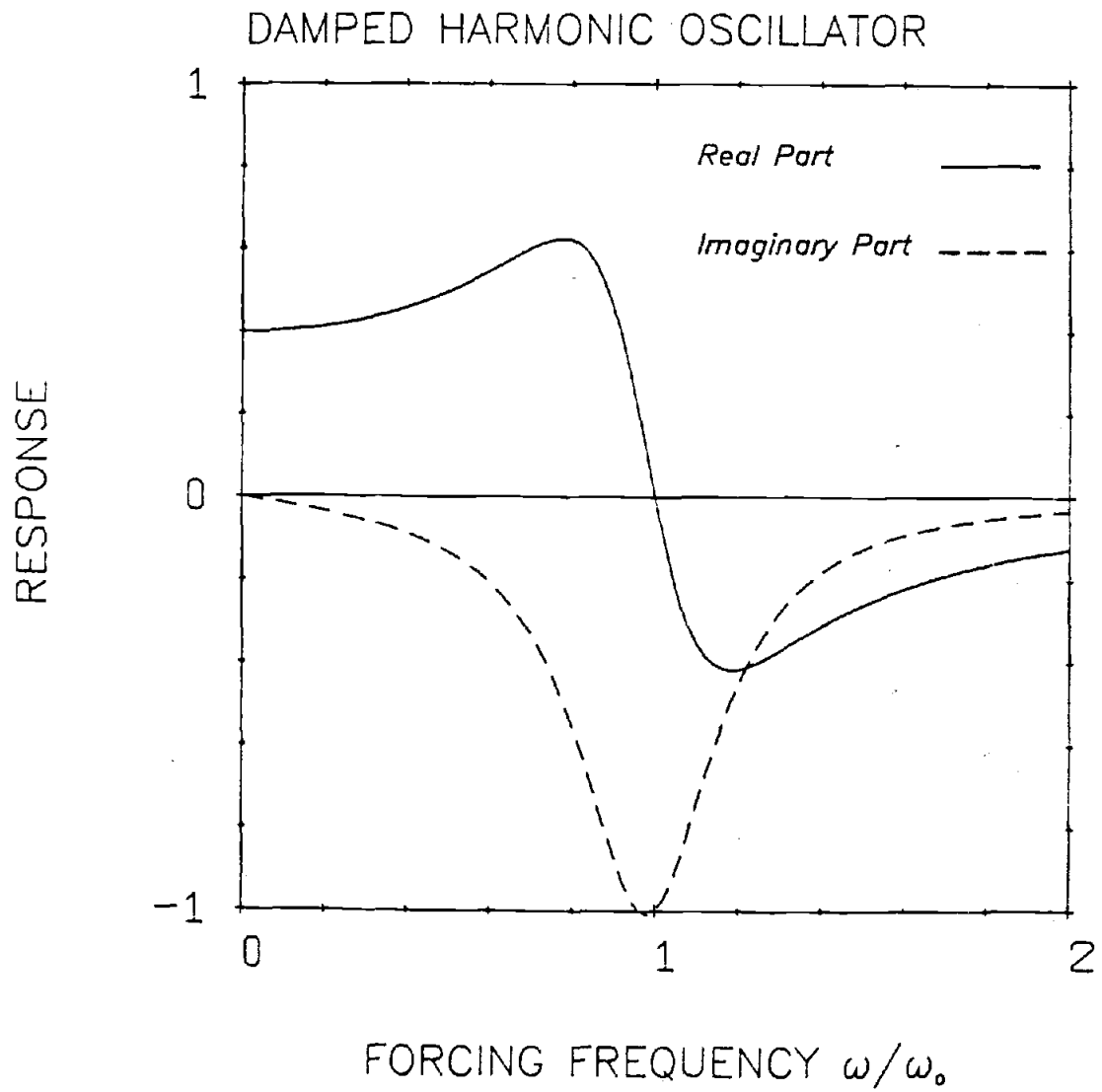


Figure 5. Schematic representation of the response of a damped harmonic oscillator to periodic forcing.

dependence of the response may be peaked near the cutoff frequencies of the various modes. Allen (1980) notes this feature of dispersive, viscous shelf models. With the parameterization of friction used by Wunsch and Gill (1976) for equatorially trapped waves, the presence of small amounts of dissipation leads to an enhanced efficiency of shelf response to atmospheric forcing at points of zero group velocity.

There are no resonances in the negative wavenumber region for positive frequency. This region corresponds to wind systems traveling in opposition to the sense of free shelf wave propagation. Again in this region the efficiency of energy transfer decreases as the forcing tends to shorter scales.

Similar conclusions to the above can be drawn for the transfer functions of horizontal components of the velocity which are not depicted here. However, whereas the transfer efficiency for sea level decays above the first mode cutoff, in the case of the velocity components the transfer functions show an increase as the inertial frequency is approached.

The influence of Ekman depth on the transfer functions is illustrated in Figure 6. Here the amplitude and phase are plotted, in the positive wavenumber region, for a fixed value of the frequency (here  $\sigma = 0.2$ ). The phase changes abruptly as each mode is crossed. The amplitude of this oscillation decreases as the Ekman depth is increased. The efficiency of the transfer is generally reduced as the frictional effect is increased. The peaks are broadened and

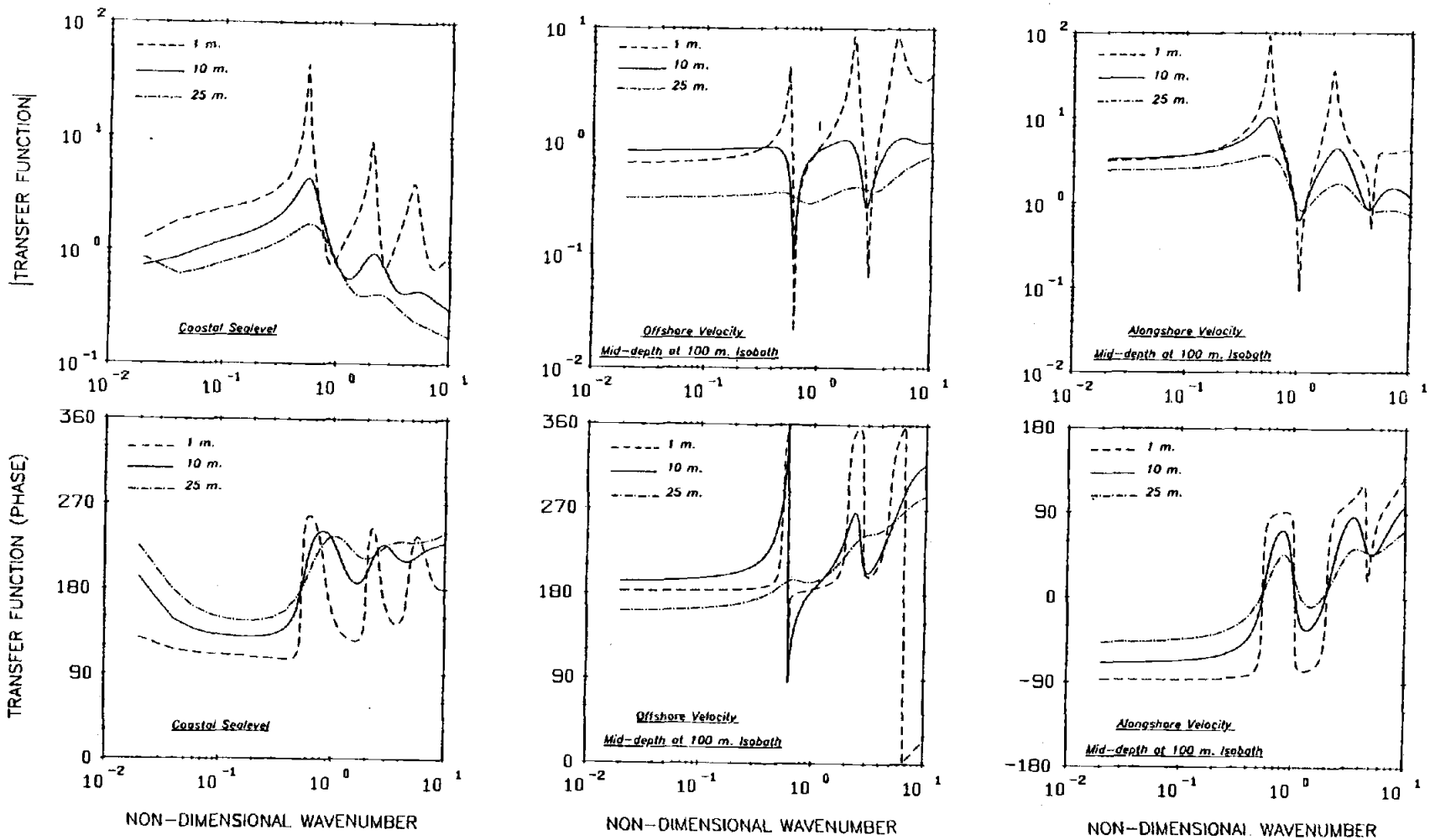


Figure 6. Transect in wavenumber of the transfer functions of coastal sealevel and the horizontal components of velocity for non-dimensional frequency  $\sigma = 0.2$

their position altered somewhat. For coastal sea level and the along-shore component of velocity the first mode is dominant and the second and third modes are further reduced in amplitude relative to the first with increased friction. This trend is reversed in the case of the offshore velocity component. Mid-depth at the 100 meter isobath was used in this discussion, but the conclusions are not changed substantially when other depths are considered.

As illustrated by Figures 3 and 4 the dispersion curves form, as it were, the skeleton of the transfer functions. The shape of these curves is modified by the choice of topographic profile or of the nearshore boundary condition. Further, as noted above, the friction parameter may alter the position of the resonances. Thus, in order to examine the effect of such changes on the model, it is not sufficient to draw comparisons at discrete points in the wavenumber-frequency plane. To avoid bias due to the shifting of the dispersion curves the transfer function is integrated at several frequencies over a range of wavenumbers. The results are essentially the model response to a wind forcing that is white in wavenumber over that range, and allow the desired comparisons. In the following section the wavenumber integration extends over the range 0.0 to 3.0 in non-dimensional units, which is believed to encompass the most important scales of the forcing, as will be discussed in Chapter IV.

#### Parameter Dependence of the Transfer Function

The influence of the nearshore boundary condition is illustrated in Figure 7. The standard topography with an Ekman depth of 10 meters

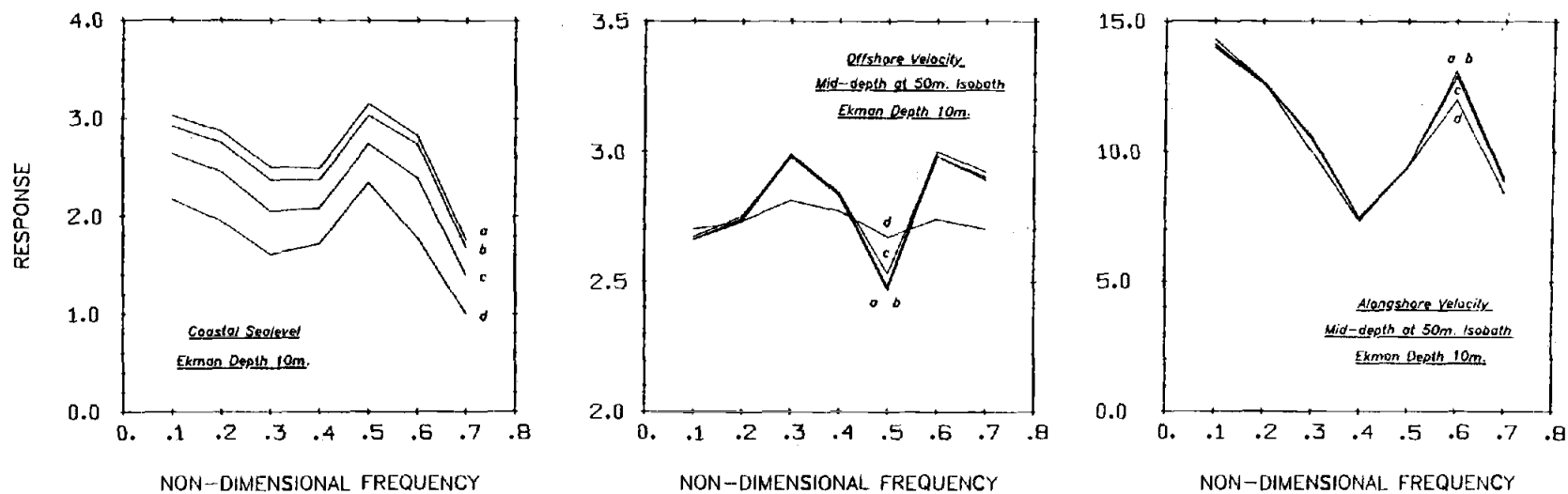


Figure 7. The influence of the nearshore boundary condition on the integrated transfer function. Curve (a) is for the regularity condition, curves (b), (c) and (d) are for no-flow with wall heights of 12, 24 and 43 meters.

is used. The velocity components at mid-depth over the 50 meter isobath are considered since this nearshore location is expected to be most influenced by the boundary condition. Curve (a) results when the regularity condition is imposed at the coast. For curves (b), (c) and (d) the no-flow condition is applied at increasing offshore distances corresponding to "wall" heights of 12, 24 and 43 meters respectively. For the offshore component, which is expected to be the most sensitive, the changes in the response amount to only a few percent until the wall height becomes considerably greater than the Ekman depth. The alongshore response is less effected. For coastal sealevel the response is merely shifted in amplitude. This reflects the spatial separation between the positions at which sea-level is evaluated. If all are computed at the same location there is again little variation from the response for the regular condition. These results lead to an important conclusion. The viscous model is insensitive to the nearshore boundary condition provided that the no flow condition, if used, has a wall height less than the Ekman layer thickness. The no-flow condition has been commonly used in conjunction with the simple exponential topography (Adams and Buchwald, 1969; Gill and Schumann, 1974) or other profiles with large coastal walls. In light of the above finding this choice may not give realistic results for an inviscid model or one employing a bottom friction parameterization of the effect of diffusion.

Now consider the effect of topographic profile on the integrated transfer function. Figure 8 illustrates the standard topography

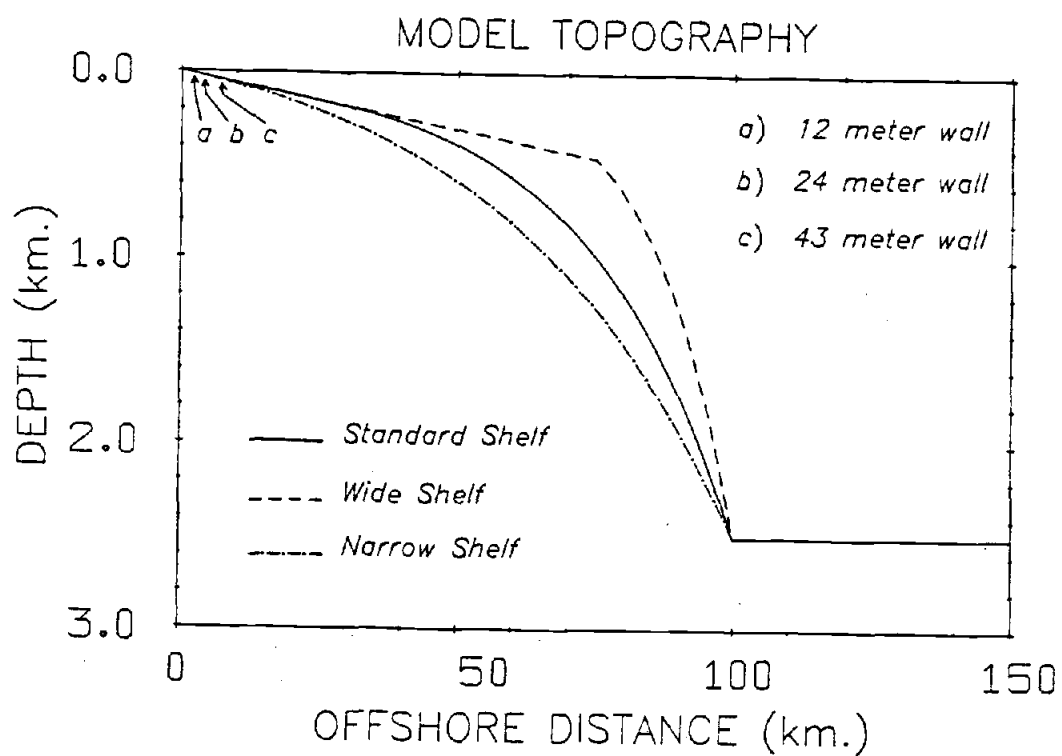


Figure 8. Alternate model topographic profiles considered for their effect on the integrated transfer function. Also shown are the wall positions of the boundary condition discussion.



together with two others used for comparison. Also indicated in the figure are the wall positions employed in the above discussion of the nearshore boundary condition. For the alternate profiles the ratio of shelf to slope width has been altered. For the wide shelf the linear region of the standard has been extended, thereby requiring a steeper slope region to attain the constant depth of the interior. The narrow shelf has the form

$$H(x) = \begin{cases} C[\exp(Dx) - 1] & , x \leq 1 \\ H_{\infty} & , x > 1 \end{cases}$$

where C and D are chosen to give the same bottom slope at the shore and interior depth as for the wide and standard profiles.

The resulting integrated transfer functions are displayed in Figure 9. The regularity condition is applied at the coast and the Ekman depth is 10 meters. At low frequencies, where the response is dominated by the longer wavelengths of the first mode resonance, the effect of profile modification is slight. At higher frequencies the response becomes highly profile dependent, though the overall range is not much altered. The shifting peaks reflect the changing location of the cut-off frequencies where, for the white wavenumber forcing of this treatment, the integrated transfer function receives a large contribution.

Finally in Figure 10 is displayed the effect of the friction parameter on the integrated transfer function. Increased Ekman layer thickness results in a general decrease of response across the sub-inertial frequency range. In particular, the peaks associated with

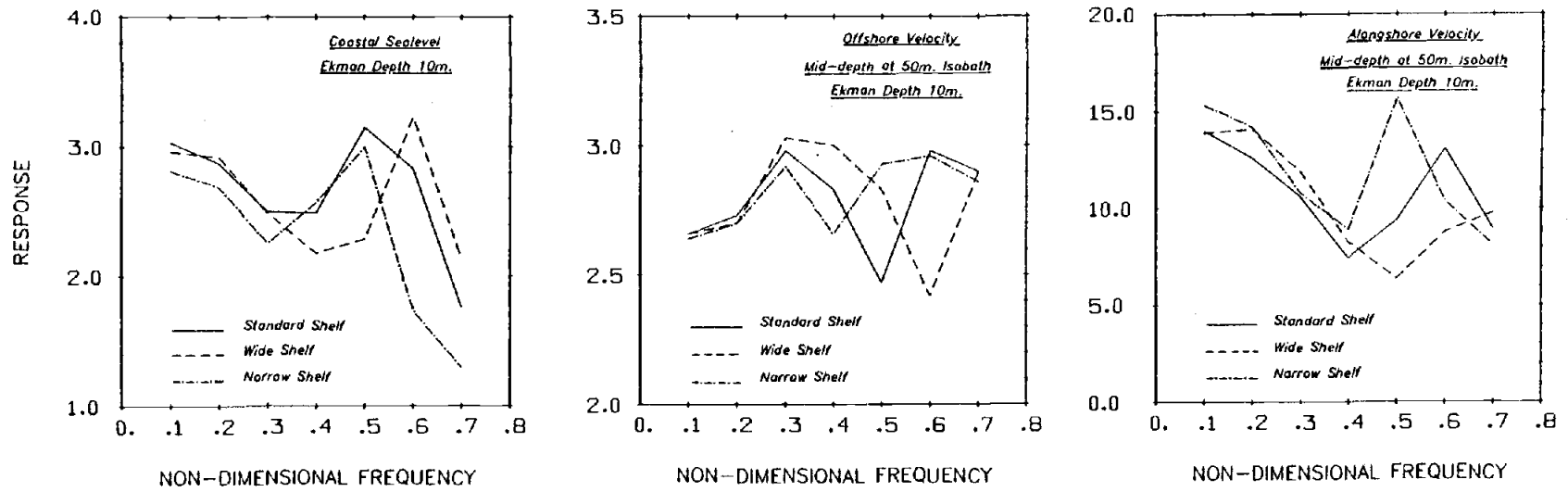


Figure 9. The effect of topographic profile on the integrated transfer function.

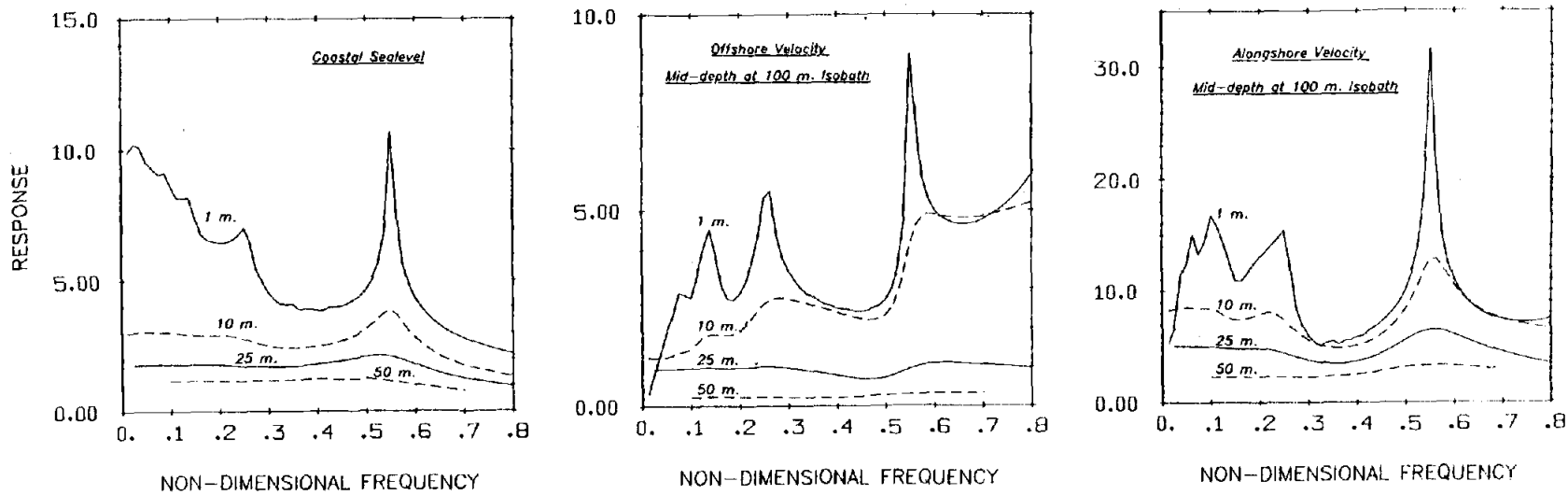


Figure 10. The influence of Ekman layer thickness on the integrated transfer function.

the cut-off frequencies are greatly reduced. For the velocity components, the reduction in the background level is less marked than for coastal sealevel, particularly when one compares the one and ten meter Ekman depths. For an actual shelf region the background response might be expected to contribute most to an observed response. The alongshore variations in topography would tend to smear out the peaks whose location is no longer fixed by a particular profile.

#### The Free Wave Solution

Before proceeding with the discussion of the forced response it is interesting to consider the homogeneous version of equations (14), (15), (15a) and (16). These represent free but viscous damped motions. If the frequency is constrained to be real and specified the result is an eigenvalue problem for a complex wavenumber  $\lambda$ . The real part of  $\lambda$  taken with  $\sigma$  gives the dispersion relation of the damped free waves. The imaginary part of  $\lambda$  is associated with the attenuation due to bottom friction.

The eigenvalue problem described above results in an attenuation length rather than a decay time. The latter formulation would require that complex frequency  $\lambda$  be the eigenvalue, corresponding to an initial value problem. Since the equations have  $\sigma$  implicit in the argument of the complex hyperbolic functions this approach is precluded.

A related problem of barotropic Kelvin waves over a flat bottom has been discussed by Mofjeld (1980). In this case the dispersion and attenuation relations can be obtained in explicit algebraic form.

Again, for the viscous free shelf wave problem we must resort to numerical means.

A simple but rather tedious method for the solution of the eigenvalue problem employs the Lindzen and Kuo (1969) method in what might be termed a Resonance Search. For a selected frequency and arbitrary forcing terms, the complex wavenumber  $\lambda$  is varied. Some convenient measure of the response, such as the absolute value of the sea level averaged across the shelf, is monitored and indicates the approach to resonance. This method was used by Wang (1976) to locate the eigenmodes of an inviscid shelf model with stratification. It is of limited use for our problem since the "search" must be conducted over two parameters, the real and imaginary parts of  $\lambda$ .

A more efficient approach is possible when the eigenvalue problem can be cast in Sturm-Liouville form. The finite difference form of the equations are expressed as

$$AZ = kZ$$

where  $Z$  is the solution vector,  $A$  the coefficient matrix and  $k$  the required eigenvalue. The eigenvalues are particularly easy to determine when  $A$  has a tridiagonal form.

For the homogeneous version of equations (14), (15), (15a) and (16) no simple eigenvalue can be identified. Indeed when the regularity condition (15a) is chosen to represent the nearshore situation, and is implemented with series expansions as described earlier, the problem does not lend itself to the matrix method. If

however the no-flow condition (15) is imposed a higher order eigenvalue problem in the wavenumber  $\lambda$  results.

$$AZ = \lambda BZ + \lambda^2 IZ \quad (25)$$

Here  $I$  is the identity matrix. This equation may be converted to a simple eigenvalue problem

$$\tilde{A}\tilde{Z} = \lambda\tilde{Z}$$

where

$$\tilde{A} = \begin{pmatrix} -B & A \\ I & 0 \end{pmatrix} \quad \tilde{Z} = \begin{pmatrix} \lambda Z \\ Z \end{pmatrix}$$

The matrix  $\tilde{A}$  composed of the submatrices  $A$ ,  $B$  and  $I$  is not tri-diagonal. Nonetheless, its complex eigenvalues  $\lambda$  may be found.

In practice a combination of the two methods was used. Because of the sparse non-tridiagonal nature of  $\tilde{A}$  the finite difference grid was of necessity rather coarse. The use of the less desirable no-flow condition is justified, provided the wall height is less than the Ekman depth under consideration. In any event, the initial estimates for complex  $\lambda$  provided by the matrix method may be refined using the resonance search method on a finer grid with the regular nearshore boundary condition.

Figures 11 and 12 illustrate the results. The dispersion diagram is in approximate agreement with that arising from the inviscid theory, displayed with the transfer function in Figure 3. The inviscid model has a high frequency cut-off for each mode where the group velocity tends to zero. The viscous dispersion curves exhibit an

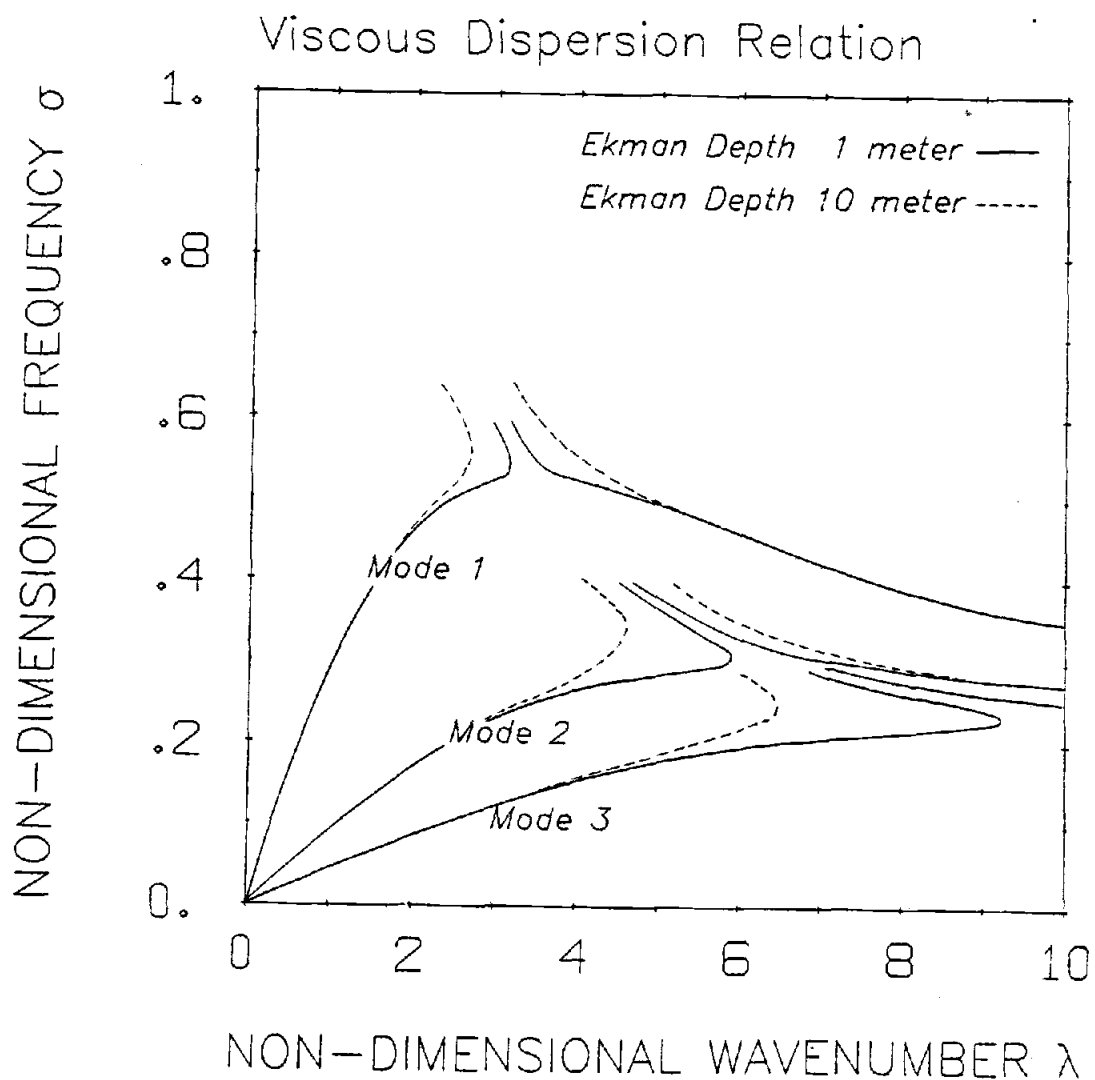


Figure 11. Dispersion relation for viscous-damped free shelf waves with Ekman depths of one and ten meters.

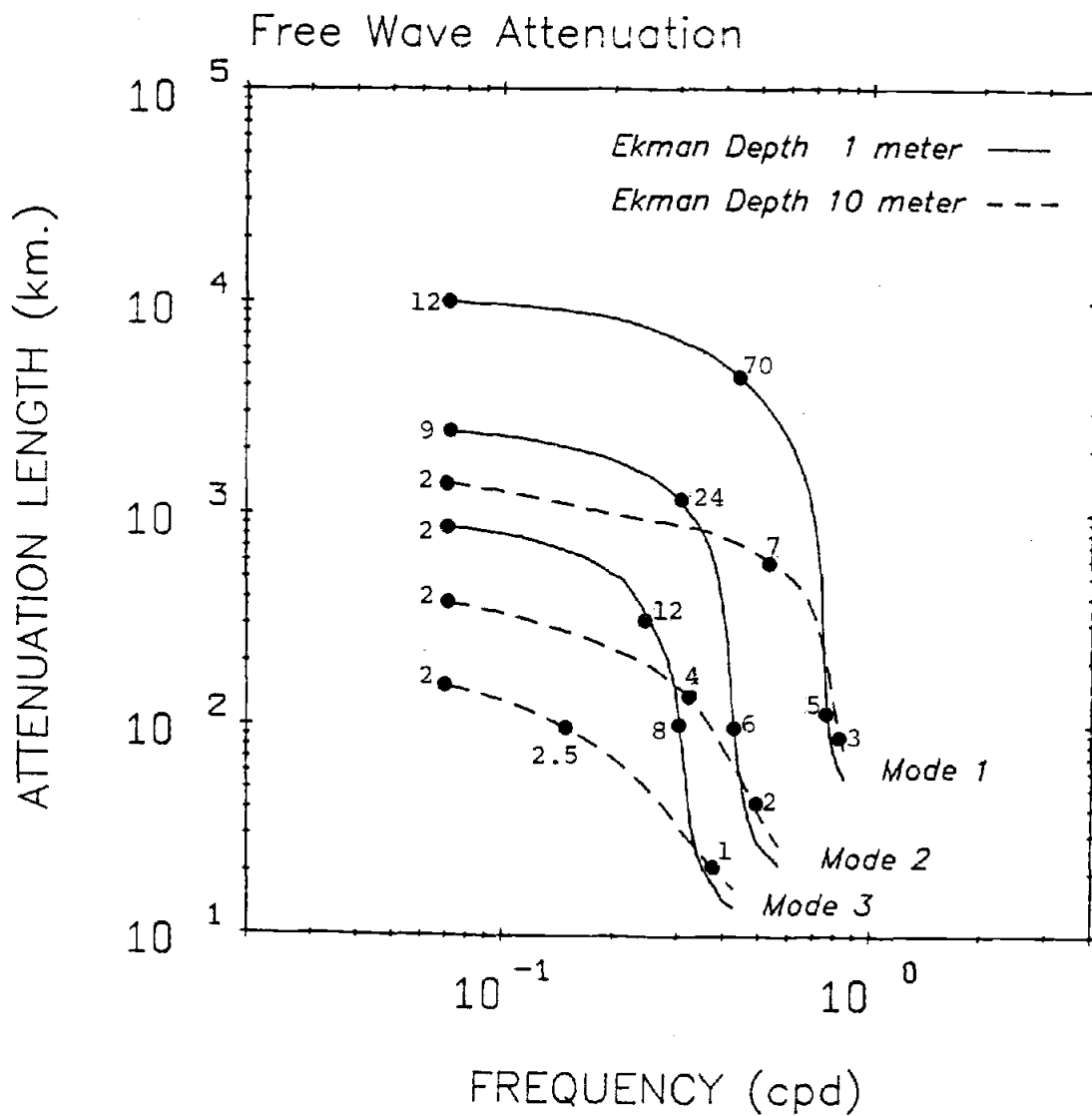


Figure 12. Attenuation characteristics of viscous-damped free shelf waves. Also indicated at discrete points is the ratio of attenuation length to wavelength.



unusual behavior in the vicinity of these cut-off frequencies. This is due to the assumption that frequency be real and wave number complex. What is thereby implied is a situation where waves forced in some region are emerging into another where they exist as free waves. This interpretation is invalid, as is the idea of attenuation length, when the group velocity approaches zero. Indeed, as shown in Figure 12, the attenuation length becomes very short in the vicinity of the high frequency cut-off and free waves cease to exist in any real sense.

Figure 12 has been drawn in dimensional units. The attenuation length (defined as the reciprocal of the imaginary part of  $\lambda$ ) decreases as the Ekman depth is increased. The attenuation lengths are not shown for points on the dispersion diagram beyond the modal peak. These values were found to essentially retrace the path leading to the high frequency cut-off, but with a sign change consistent with the reversed direction of energy propagation. The numbers indicated at discrete points on each curve are the ratio of the attenuation length to the wavelength. For each curve this begins low at the long wave - low frequency end, increases to a maximum, then decreases sharply in approaching the high frequency cut-off.

A commonly observed feature of continental shelf studies is that the coherence of the coastal response to atmospheric parameters has a banded structure. Peaks of coherence often coincide with the cut-off frequencies of the lower few shelf modes. This behavior was noted by Brooks (1978) for sea level off the North Carolina coast.

The explanation often tendered for this phenomenon is that, with zero group velocity, the forced energy is dispersed only by mean advection and dissipation and thereby tends to persist in these frequency bands. The results of this section suggest another explanation. The coherence between locally forced fluctuations, such as sealevel or current, and their forcing agency is reduced in the presence of free waves. The latter owe their origin to forcing distant in space and time. Since attenuation reduces the contribution of free waves an enhanced coherence is to be expected whenever such attenuation is particularly severe. Thus, based on Figure 12, free wave contamination of the locally forced signal is expected to be at a minimum near the cut-off frequencies. Further, free wave activity should decrease with increasing mode number.

#### IV. DATA ANALYSIS AND MODEL INTERCOMPARISON

In this chapter we analyze the available data for the Oregon shelf with a view to forming a comparison with the predictions of the viscous forced model. The Pacific coast of the northwest United States is a suitable region for this comparison. The coastline is approximately straight and the submarine topography approximately uniform in the alongshore direction. A substantial data base exists for the region from a variety of field studies during the past decade or so. Kundu, Allen and Smith (1975) have shown using empirical eigenmode analysis that, at subinertial frequencies, barotropic disturbances are the major response to the alongshore component of windstress, as indeed theory predicts for this mid-latitude location (Romea and Allen, 1980).

##### Data Description

The data utilized in this study are summarized in Table 1 and Figure 13. A continuous record of wind speed and direction exists for Newport, Oregon for the ten year period 1969-78. The location and characteristics of the wind recorder are described by Frye (1972).

Wind stress is computed from the speed and direction using the quadratic drag law

$$(\tau^x, \tau^y) = \rho_a C_D |\vec{W}| (U_w, V_w)$$

where  $\rho_a$  is the density of air,  $\vec{W} = (U_w, V_w)$  the wind velocity and  $C_D = 1.5 \times 10^{-3}$  is the drag coefficient. For the Oregon coast the north-south component of wind stress is identified as alongshore,

Table 1. Summary of Oregon shelf data used in the computation of the wind-coherent response

Variable	Measured at	Record Duration	Comments
Sealevel	Newport, Oregon	Jan. 1969 - Dec. 1978	Measured within Yaquina Bay
Wind	Newport, Oregon	Jan. 1969 - Dec. 1978	
Atmospheric Pressure	Newport, Oregon	Jan. 1973 - Dec. 1978	
Horizontal Currents	NH - 15	Aug. 8 - Oct. 29, 1972	60 meter instrument
	Poinsettia D	Jun. 28 - Aug. 4, 1973	60 meter instrument
	Carnation	Jun. 30 - Aug. 28, 1973	60 meter instrument
	Forget-me-not	Jul. 22 - Aug. 27, 1973	60 meter instrument
	Sunflower A	Jan. 28 - Apr. 26, 1975	75 meter instrument
	Sunflower B	Apr. 28 - Jul. 28, 1975	75 meter instrument
	Sunflower C	Jul. 29 - Sep. 12, 1975	75 meter instrument

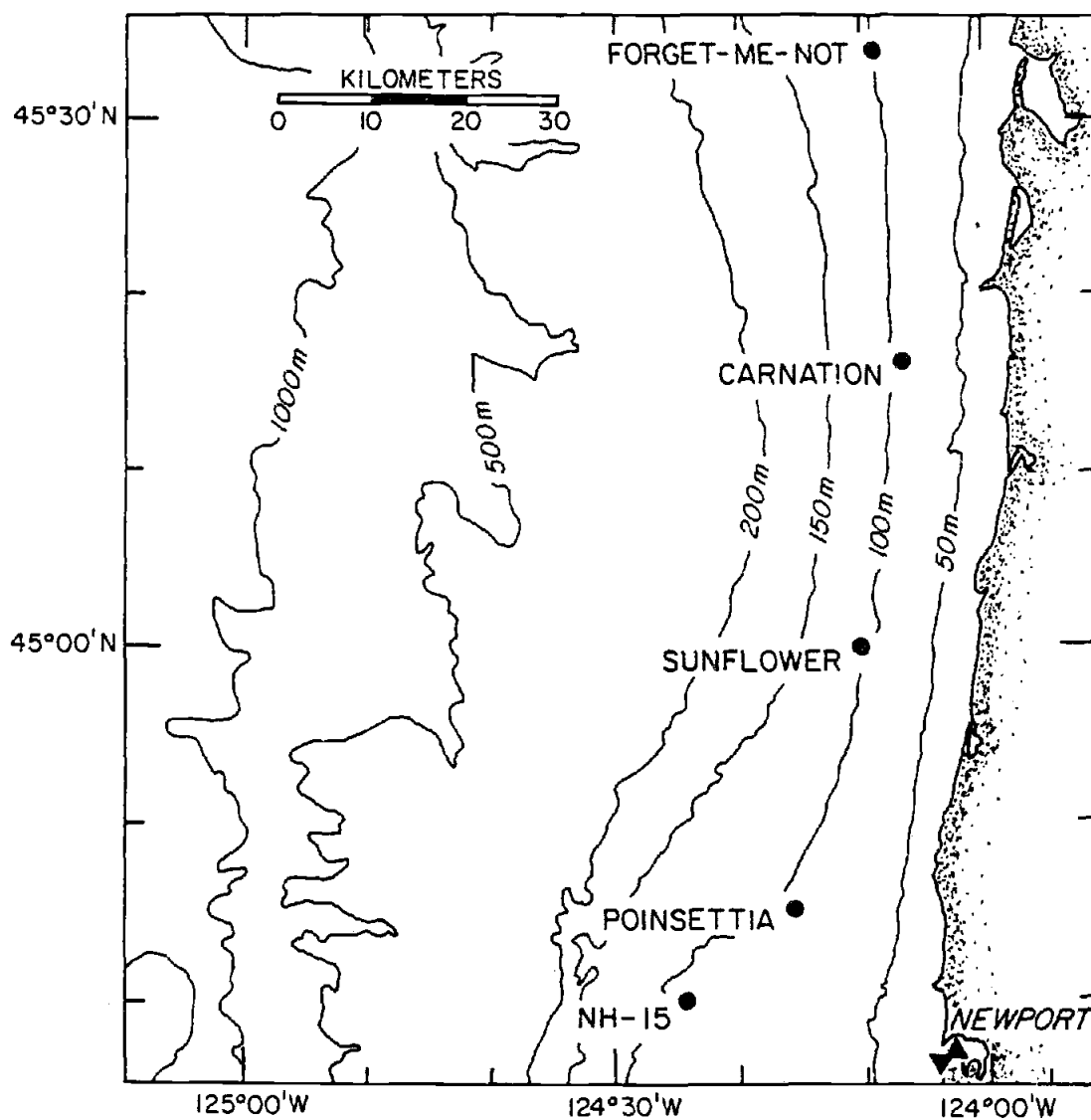


Figure 13. Location of the current meter moorings used in this study.

since this is the basic orientation of the topography.

A record of sea level at Newport covers this same period. The tide gage is located within the Yaquina Bay, approximately one nautical mile from the open ocean. The atmospheric pressure data required to form the adjusted sea level only exists for the latter six years of the period covered by the wind and tide gage records.

Current recording instruments have been deployed off the Oregon coast in a number of field experiments. The instruments were placed at a variety of positions and depths as described in the data reports of Pillsbury et al. (1974a, 1976b) and Gilbert et al. (1976) for the CUE I, CUE II and WISP/UP75 experiments respectively.

In dimensional terms the viscous model was implemented in the frequency range 0.02 - 1.13 cpd. No single current meter installation is of sufficient duration to provide reliable cross spectral estimates over this entire range. Instead, we combine all available records of mid-depth current meters at the 100 meter isobath. This combination has the greatest coverage. The resulting ensemble, with data from three separate years, is only one fifth the length of the sea level record and will, as a result, provide a less reliable comparison with the model.

All of the data described above were available as hourly time series.

#### Data Analysis

The inertial period at these latitudes is approximately 17 hours (1.4 cpd). Thus, the subinertial frequency range overlaps the

diurnal tidal band, which may contain considerable energy for some variables. In particular, the sea level data has strong diurnal ( $O_1$ ,  $K_1$ ) and semi-diurnal ( $M_2$ ,  $S_2$ ) tidal peaks. We seek to reduce these peaks, since in the spectral analysis their energy may leak into adjacent frequency estimates.

It is not feasible to eliminate the tidal peaks by band-pass filtering. Instead, using the method of Munk and Cartwright (1966), a fit is made to the tides. The residual series from this fit has a much reduced contribution from the diurnal and semidiurnal tides. This is seen in Figure 14, where the ten year ensemble average of winter autospectral estimates is shown for the original data and the residuals from the Munk-Cartwright fit. The sea level data is filtered and decimated to a three-hourly series prior to the tidal removal. The low-pass filter used has a half-power point at 3.6 cpd and rolls off over a 1.44 cpd interval. This filtering and decimation is applied to all other data.

Leakage of the remaining energy in tidal peaks is further minimized in the subsequent spectral analysis by applying the Finite Fourier Transform to data segments of 29 day duration. For this series length Fourier frequencies lie close to all major tidal peaks.

The sea level residuals and the atmospheric pressure data are combined to form the adjusted sea level for the six years 1973-78. Each millibar of pressure change results in a one centimeter adjustment of sea level.

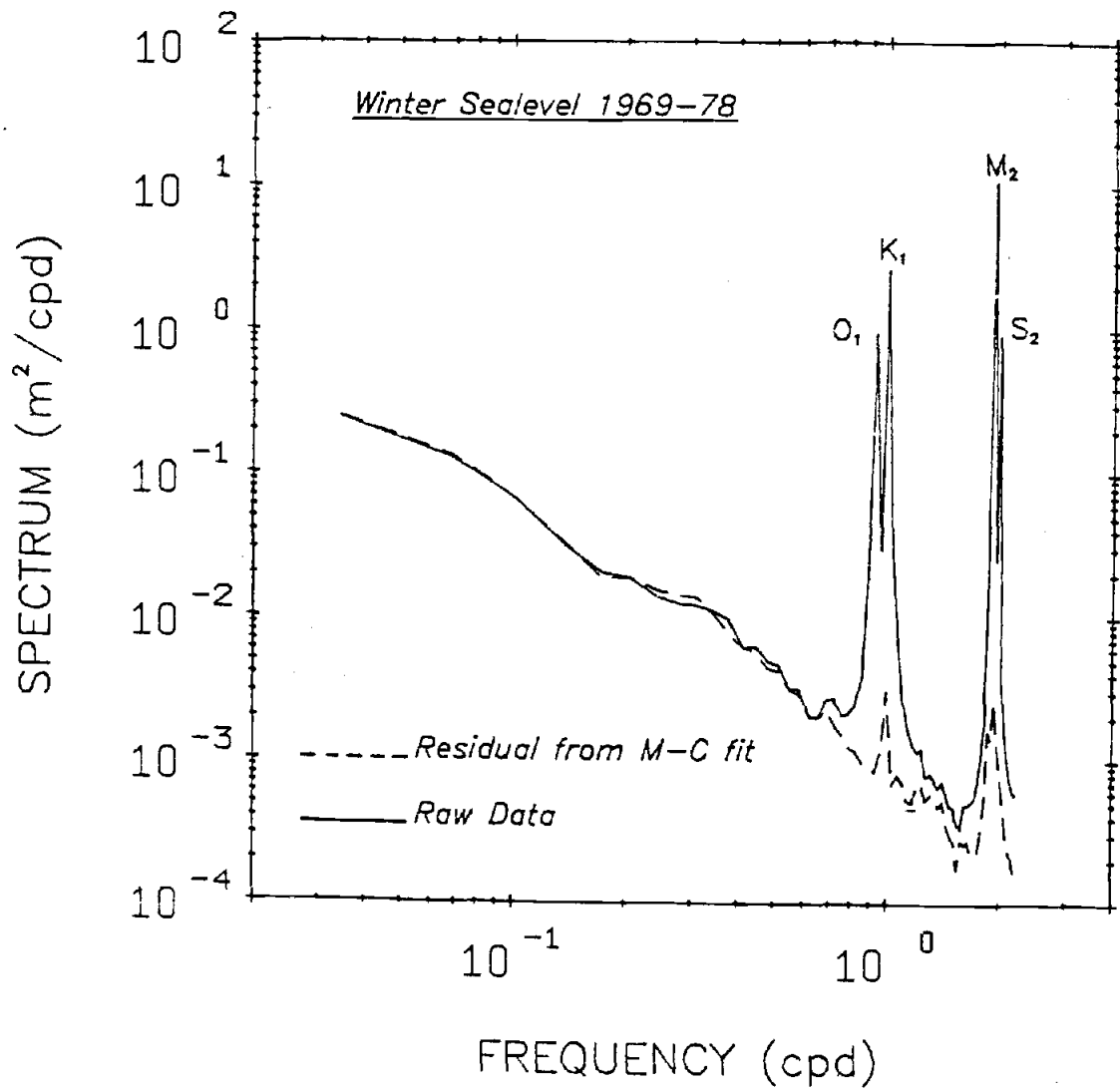


Figure 14. Reduction of the tidal component of sealevel using a Munk-Cartwright fit.



The time series of sea level and of the meteorological variables display a marked seasonal cycle. The amplitude of low frequency fluctuations is far greater in the winter months than in the summer. This may be seen in Figure 15 where, for a typical year 1975, the seasonal cycle in the behavior of adjusted sea level and the wind stress is evident. The figure also shows a visual correlation between events in the wind and those in sea level and the alongshore velocity at the Sunflower mooring.

The seasonal cycle is also seen in the autospectral estimates computed from each 29 day segment. For each variable these have a bimodal distribution. The degree of non-stationarity is quantified with a test developed in Appendix B. Figure 16 displays the results of the test for the six years of adjusted sealevel. Based on the hypothesis that the spectral estimates are drawn from a stationary population, the Type I error represents the probable error incurred if this hypothesis is rejected. Small Type I errors thus correspond to a high degree of non-stationarity in the data. The adjusted sea-level is seen to be highly non-stationary in much of the subinertial frequency range. The situation is improved when the spectral estimates are divided between "winter" and "summer" seasons. Based on the stationarity test the best definition of summer is found to be May through October, winter being the remaining months. This subdivision of the year is consistent with the seasonal transitions commented on by Sobey (1977).

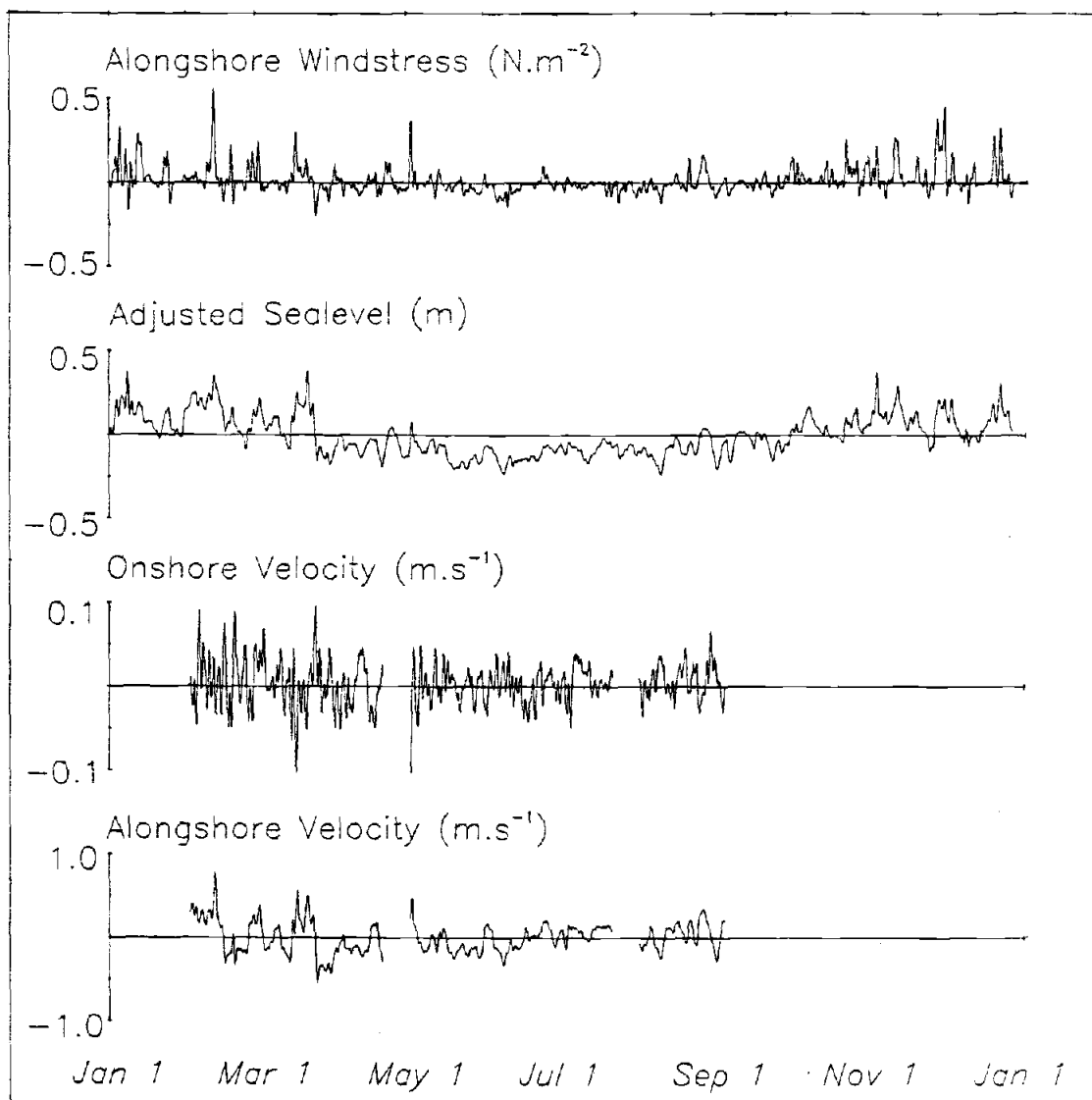


Figure 15. Time series of alongshore windstress, adjusted sealevel and current from the Sunflower site for the year 1975.

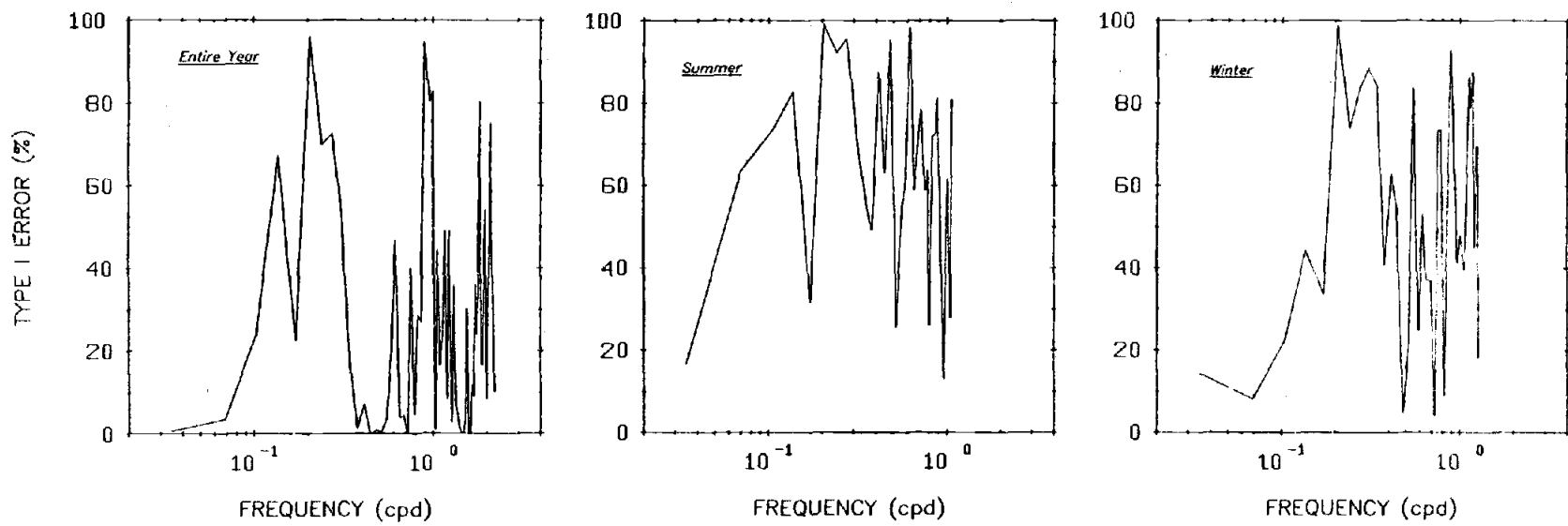


Figure 16. Stationarity test for six years of adjusted sealevel at Newport, Oregon. 1973-1978.

The ensemble averaged autospectra for uncorrected sea level, adjusted sea level, alongshore wind stress and atmospheric pressure are displayed in Figure 17. The necessity for separate treatment of winter and summer data is evident.

As seen in Table 1, the current meter data is drawn primarily from the summer months. In view of the sparseness of this data, no attempt was made to form separate ensembles by season. Nor is it possible to use any form of orthogonal mode analysis to extract the barotropic component without further depleting the record length. Instead, the longest mid-depth record was selected for each mooring. Whenever adjacent records in the vertical exist, a visual inspection of the data reports confirms the approximate barotropic nature of the fluctuations.

At each location the local alongshore axis is chosen from the progressive vector diagram and the local bathymetry. Each set of current meter observations is rotated into its appropriate frame. The co-ordinate rotations used are listed in Table 2.

#### The Coherent Response of Sea Level to the Wind

We now compute, from the spectral estimates of the adjusted sea level and wind stress, the coherent response defined in equation (18). Separate ensembles are formed for the winter and summer data. In view of the marked seasonal differences in the autospectra, as well as in the meteorological and hydrographic regimes that exist, the close agreement of the estimates of coherent response for both seasons

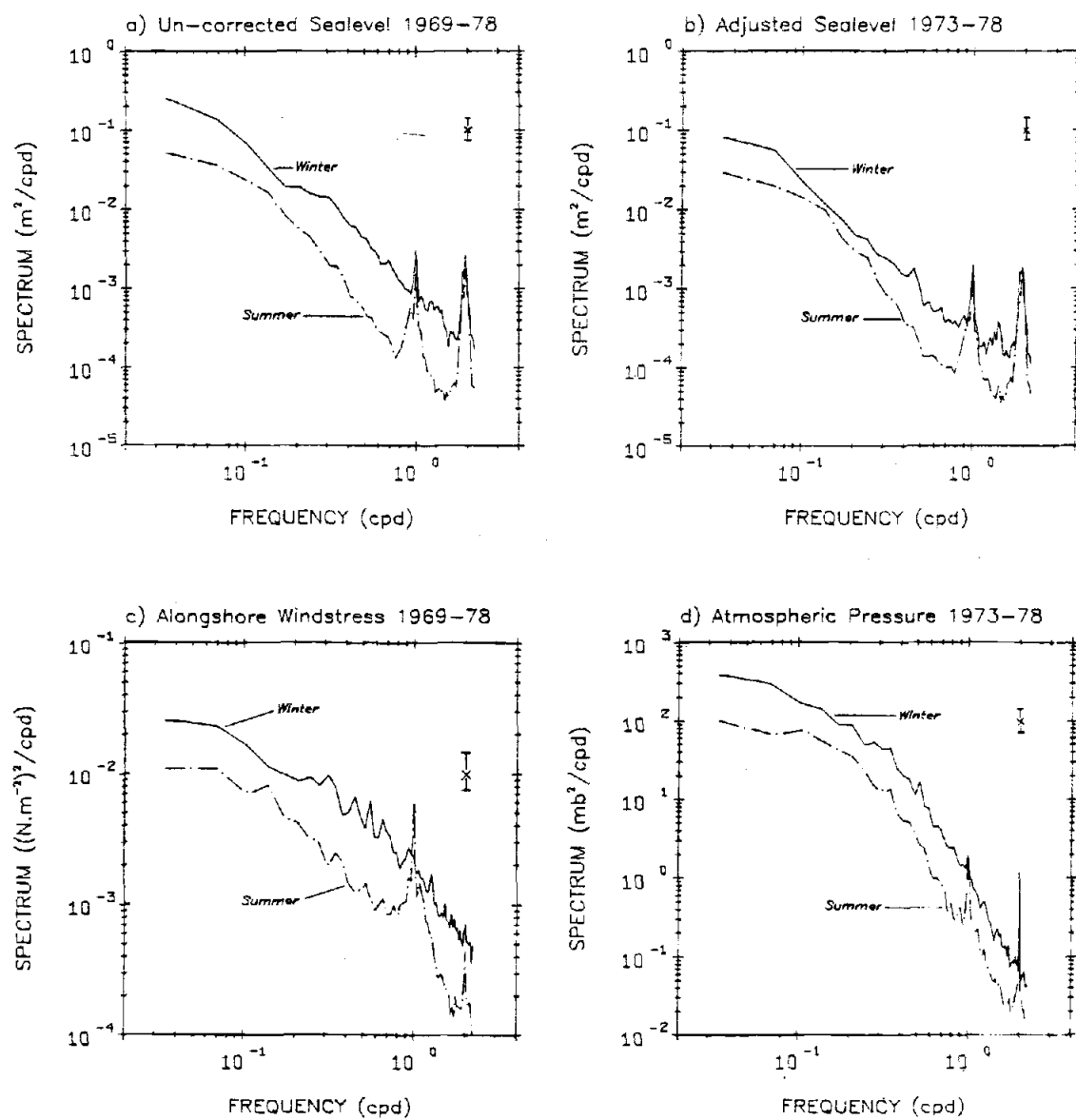


Figure 17. Ensemble averaged autospectra for summer and winter seasons. The 95% confidence ranges are shown in the upper right hand corners.

Table 2. Rotation angles (positive clockwise) of local topographic axes for each current meter mooring, and spatial separations from Newport, Oregon.

Station	Angle	Separation(km.)
NH-15	15 <sup>0</sup>	30
Poinsettia	15 <sup>0</sup>	25
Carnation	0 <sup>0</sup>	75
Forget-me-not	0 <sup>0</sup>	110
Sunflower	8 <sup>0</sup>	45

shown in Figure 18 are remarkable. For contrast the coherent response for the uncorrected sea level is shown in Figure 19. Here sea level has not been adjusted for the effect of atmospheric pressure as an inverse barometer and the seasonal differences seen in the autospectra carry over into the squared coherence, the coherent response and the phase. It would appear that while atmospheric pressure can cause a substantial response in sea level, its effect is basically isostatic in the case of the Oregon shelf.

In view of the above result, it seems that the simplified forcing assumed for the model is justifiable at least in the case of coastal sea level response. Later we shall attempt to compare model predictions of response and phase with those produced above for the adjusted sea level.

#### The Coherent Response of Horizontal Currents

The cross-spectral analysis is next applied between the alongshore and onshore components of velocity (from which the tidal constituents have not been removed) and the alongshore wind stress. The alongshore component yields reasonably stable estimates for the coherence, even though the data records are drawn from points with varying spatial separations from the wind recorder (see Table 2). The coherence between the onshore component and the wind is much poorer. Only for a few frequencies are the coherences in excess of the 90% significance level, even when bandaveraging is added to the usual ensemble average. In Figure 15 the onshore velocity fluctuations were seen to be almost an order of magnitude less than those

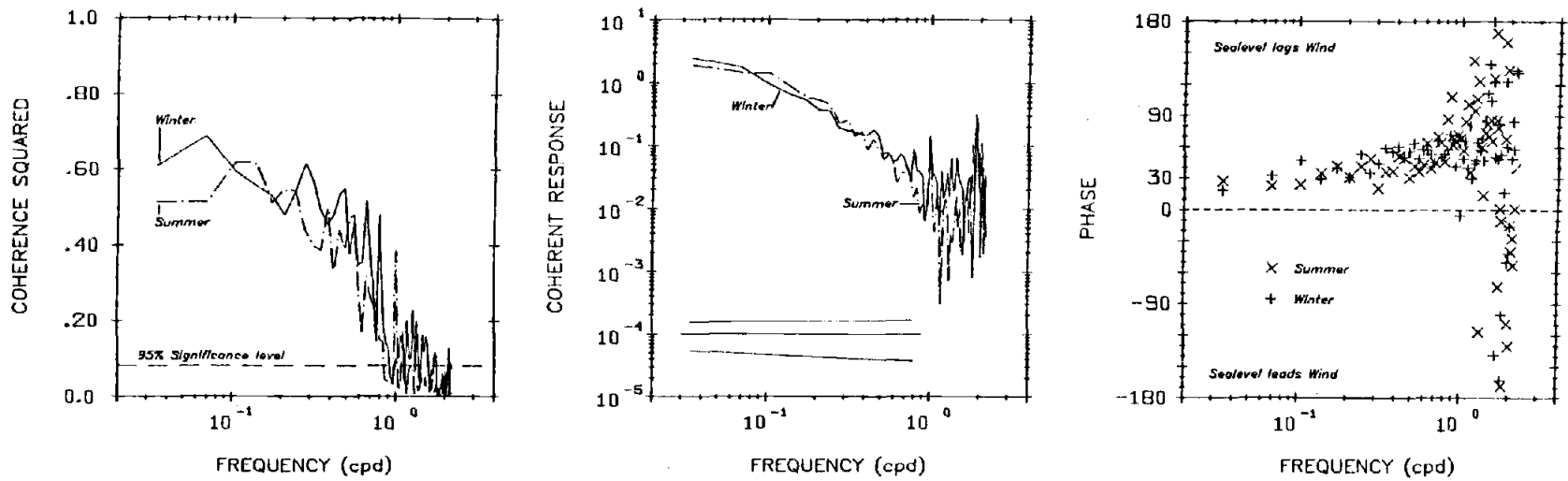


Figure 18. The coherent response of adjusted coastal sealevel. 1973-1978 with the estimated 95% confidence range.



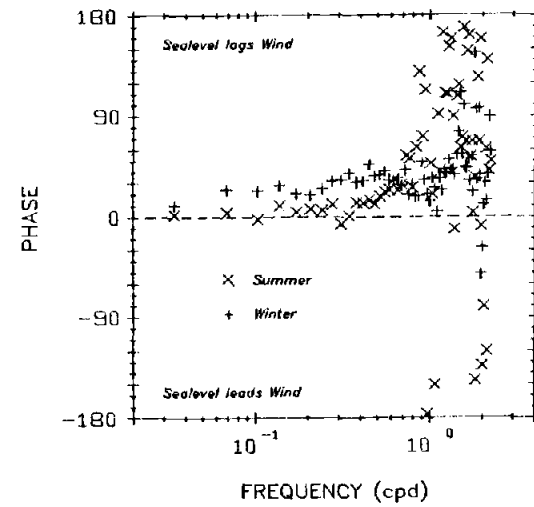
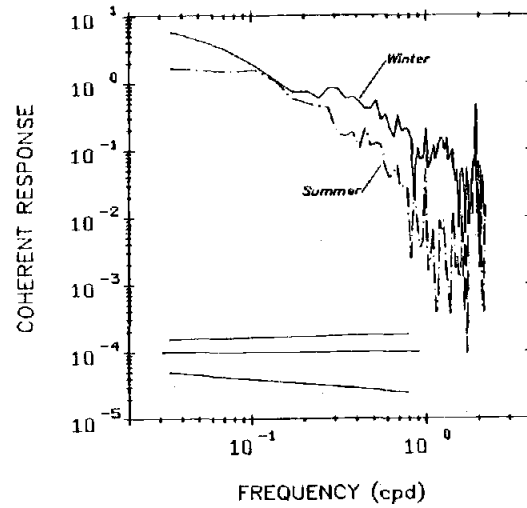
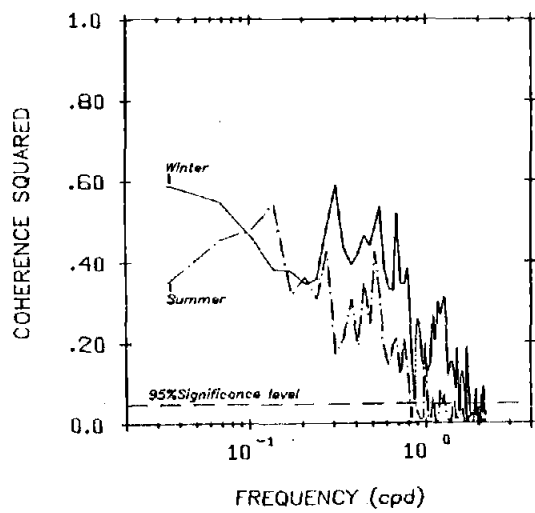


Figure 19. The coherent response of un-corrected sealevel, 1969-1978.

in the alongshore direction and only for the largest wind events is any visual correlation evident.

The autospectra of the horizontal velocity components are shown in Figure 20. Their coherent responses are discussed in the next section where a comparison with the model response is attempted.

### Intercomparison of Model and Experiment

The model response to alongshore wind stress is now computed using the transfer functions defined in Chapter II. With the assumption that the wave number-frequency spectrum of the wind may be decomposed as in Equation (23) the model response may be computed from Equation (24). The phase is determined as the argument of the complex integral in (24).

The wave number dependence of the wind is modelled by the basic power law form

$$S_1(\lambda) = \begin{cases} K|\lambda|/\lambda_0 & , \lambda \leq \lambda_0 \\ K(|\lambda|/\lambda_0)^\alpha & , \lambda \geq \lambda_0 \end{cases}$$

Here  $\alpha$  is the exponent of the power law and  $\lambda_0$  a wave number below which the spectrum falls off to zero. The scale factor  $K$  is chosen to normalize the integral of the wave number spectrum to unity as assumed in (24) and is thus not a free parameter.

Values of  $\alpha$  in the range -2 to -3 are indicated by the available wave number information on wind spectra, for example Julian and Cline (1974), and by theories of two-dimensional, quasi-geostrophic turbulence (Kraichnan, 1967). Such power laws have been employed by Frankignoul and Muller (1978) to represent windstress forcing in

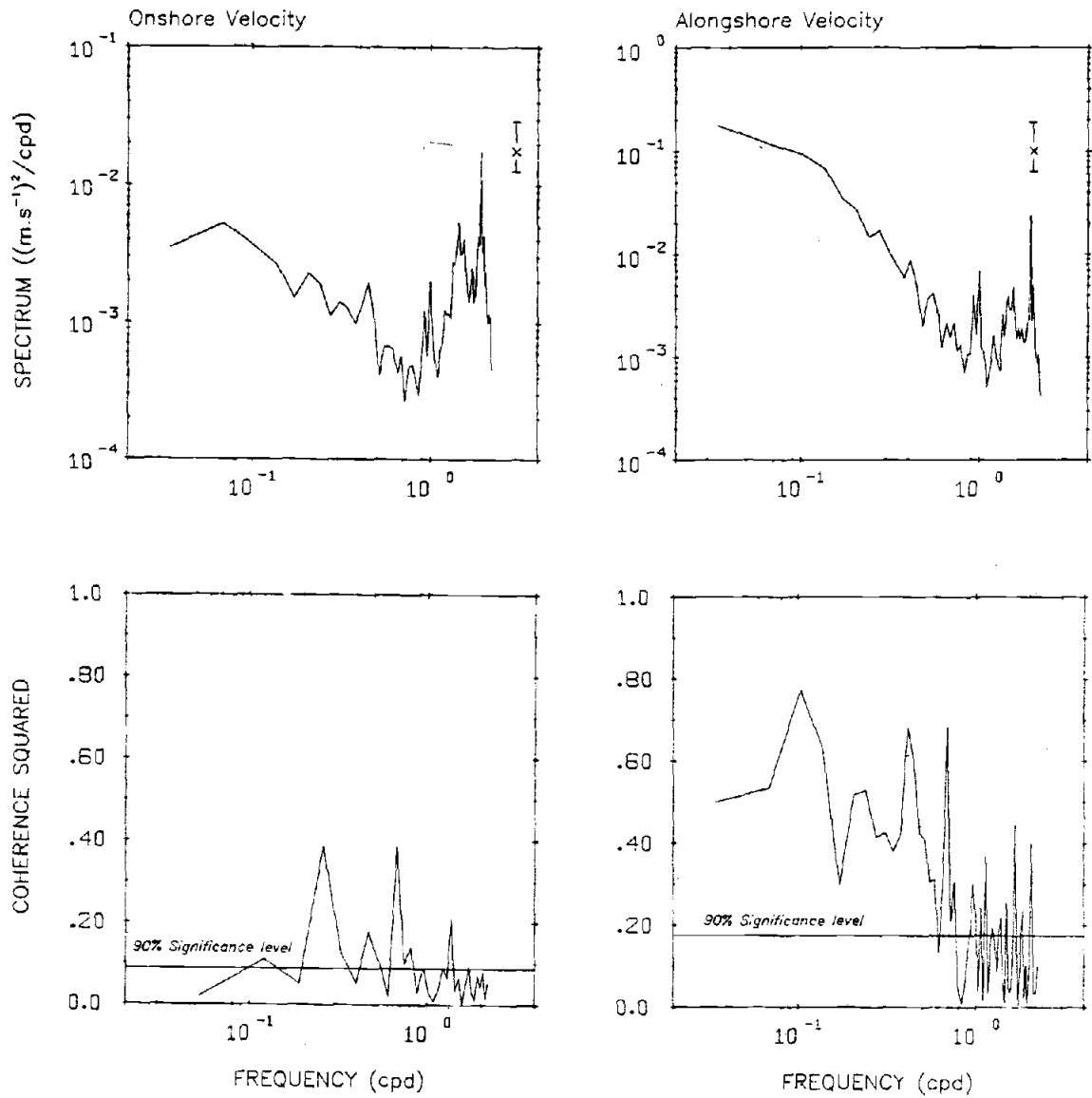


Figure 20. Ensemble averaged autospectra and coherences with the alongshore wind stress for the horizontal components of velocity.

mid-ocean. Kinetic energy in the atmosphere is found to peak at scales of the order of 5,000 kilometers, thereby suggesting a suitable value for  $\lambda_0$ .

The transfer functions computed in Chapter III span the non-dimensional wave number range 0.02 to 10.0. These correspond to scales of approximately 8000 and 15 kilometers, respectively. For the latter scale, the assumption of no across shelf variation in the windstress is unlikely to be valid. However, with an inverse square to inverse cube power law, the high wave number regions make little contribution to the numerically evaluated response integrals.

The model responses discussed below are based on an inverse square power law with  $\lambda_0 = 0.02$  (8000 km scale). The complete transfer functions were only evaluated for Ekman depths of one and ten meters. In general, the model response is more sensitive to changes in the friction parameter than to the  $\alpha$  and  $\lambda_0$  parameters when these are held in the ranges suggested above. In view of the length of the data record available and the resulting stability of the spectral estimates, the model fit should likely be biased toward agreement with the adjusted sealevel response. For this purpose the summer and winter results in Figure 18 have been combined in a single ensemble. In Figure 21 we see that for an Ekman depth of one meter the model response is in close agreement with the coherent response from data. With increased friction (ten meter Ekman depth) the coherent response is considerably underestimated, though the shape is well reproduced. For the phase the ten meter Ekman depth model

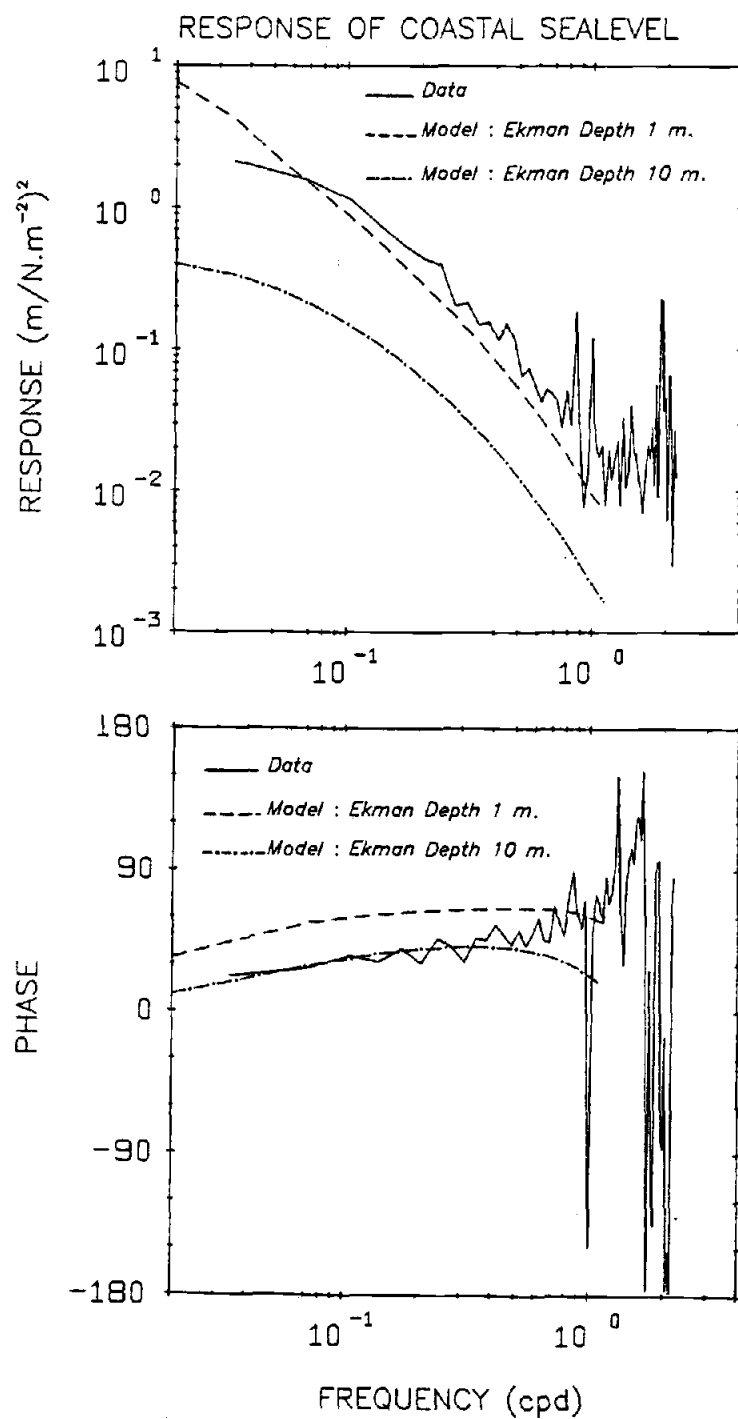


Figure 21. Model fit to the coherent response of adjusted coastal sealevel.

is in closer agreement with the data than is the one meter case.

Figure 22 shows the fit to the coherent response of the horizontal currents. For the onshore component, only those estimates based on coherence significant at the 90% level are displayed. The ten meter Ekman depth appears to give a better fit for both response and phase than the one meter Ekman depth case. However the data, particularly the onshore component, have broad uncertainty ranges. Those indicated have been estimated at the 90% level. The spectral estimates for the onshore and alongshore components have 52 and 26 degrees of freedom respectively. In the case of the onshore component, bandaveraging by two was used in addition to the ensemble average over the thirteen available 29 day segments. It appears that the model is in reasonable agreement with field data for Ekman depths of between one and ten meters.

In the next sections we examine some further properties of the model, using the above representation of the wave number dependence of the wind field.

#### Cross-Shelf Phase Differences

A feature of some field studies is that phase differences exist between flow variables measured at points separated in off-shore position. Fluctuations nearshore lead those farther offshore, as observed by Sobey (1977) for the Oregon shelf and by Brink, Allen and Smith (1978) off Peru.

Phase differences of the correct sign are predicted by the viscous long-wave model of Brink and Allen (1978). Here viscosity is

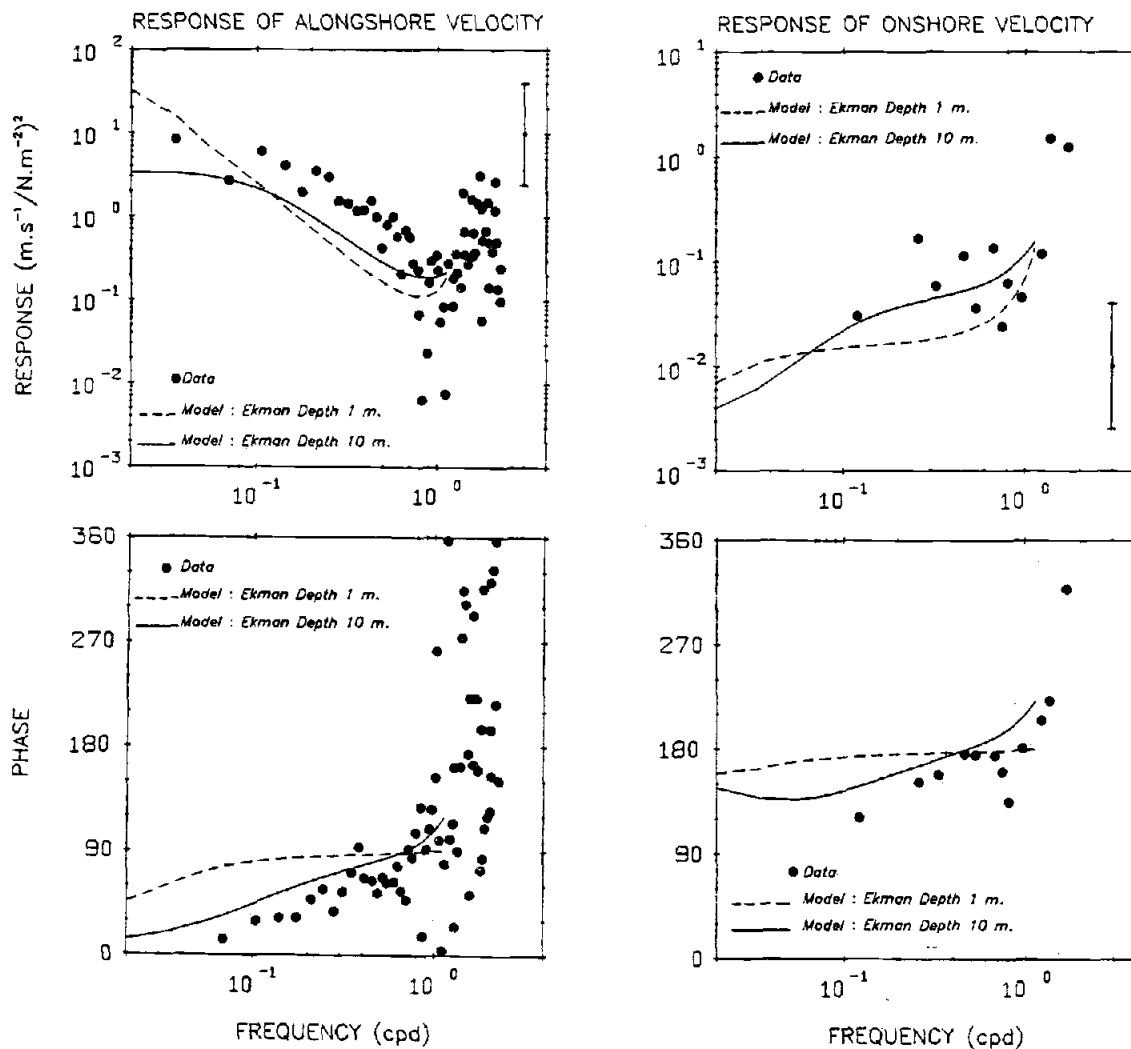


Figure 22. Model fit to the coherent response of horizontal currents at mid-depth over the 100 meter isobath. The estimated 90% confidence ranges are indicated. For the onshore component only estimates based on coherences significant at the 90% level are displayed.

parameterized through a bottom friction coefficient. Ekman layer dynamics are used by Mofjeld (1980), in a study of barotropic Kelvin waves in a coastal zone of constant depth, and cross-shelf phase differences also arise.

Such phase differences are evident in the model responses of horizontal velocity components produced in this study, as illustrated in Figure 23. Here the response functions, based on the wavenumber structure for the wind assumed in the previous section, are computed for mid-depths at the 25, 50, 75, 100, 150, 200 and 500 meter isobaths. Curves (a) and (b) correspond to a non-dimensional frequency of 0.20 (3.5 day period) while curves (c) and (d) are for 0.55 (1.3 day period). The response for the former frequency is dominated by the long wave, non-dispersive portions of the modes while the latter frequency is chosen to represent the cut-off frequency of the first mode. For curves (a) and (c) a ten meter Ekman depth is used while for curves (b) and (d) the Ekman depth is one meter. The results have been converted to the coordinate system commonly used for the Oregon situation; U is onshore and V is to the north.

For the alongshore component the phase lag of current to the wind is seen to increase offshore. The range of variation is far greater in the case of the ten meter Ekman depth than for the one meter case, which departs only slightly from the  $90^\circ$  phase lag predicted by the inviscid theory.

In the case of the onshore component the phase lag increases with offshore distance for the one meter Ekman depth. With a ten



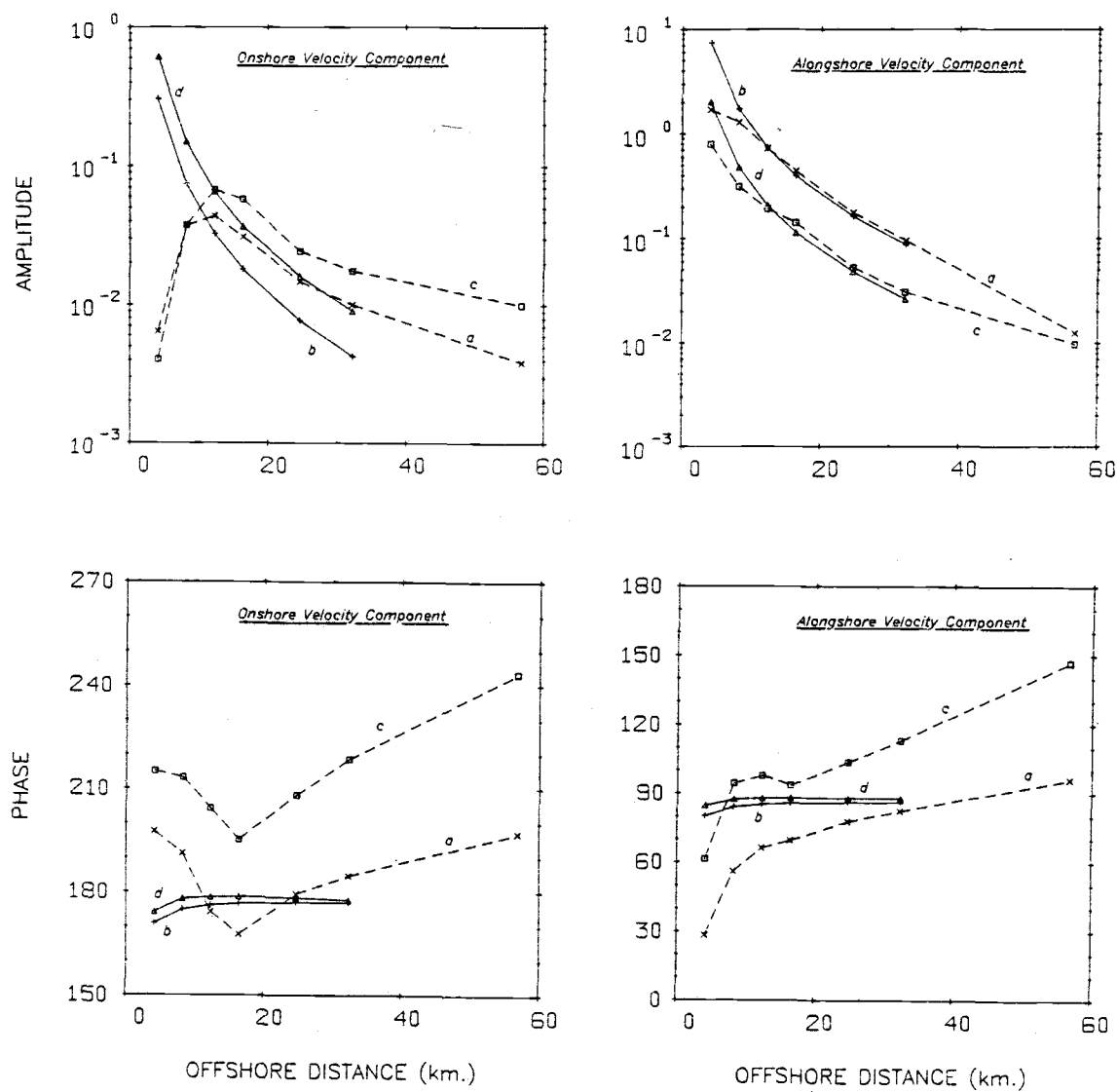


Figure 23. Cross-shelf variation in model phase and response amplitude. Curves (a) and (b) are for  $\sigma = 0.2$ , curves (c) and (d) for  $\sigma = 0.55$ . For (a) and (c) the Ekman depth is ten meters, for (b) and (d) one meter.

meter Ekman depth the phase lag is at a minimum at an offshore distance of approximately 16 kilometers and increases both inshore and offshore of this position.

Also shown in Figure 23 are the amplitudes of the model response. When the water depth is sufficient that the water column be largely inviscid, the alongshore velocity response is insensitive to Ekman layer thickness. However, in the nearshore region increased friction causes a reduction of the response of the alongshore velocity.

For the onshore velocity component the response amplitude is more sensitive to the Ekman depth. For the ten meter case the current peaks at an offshore position close to that at which the phase lag to the wind was minimized. A similar behaviour occurs with the one meter Ekman depth inshore of the shallowest (25 meter) location shown in Figure 23.

#### Balances in the Continuity and Horizontal Momentum Equations

Again using the power law wavenumber dependence of the wind, the mass and momentum balances may be discussed in terms of the appropriate model response functions.

In Figure 24 the responses of  $U_x$  and  $V_y$  are shown for mid-depths at the 50, 100 and 200 meter isobaths. Ekman depths of one and ten meters are used. The importance of  $V_y$  relative to  $U_x$  in the balance generally decreases as frequency increases and drops rapidly beyond the cut-off frequency of the first mode (0.75 cpd). As the shoreline is approached, the balance becomes increasingly confined to the x-z plane, particularly for the case of the ten meter Ekman layer

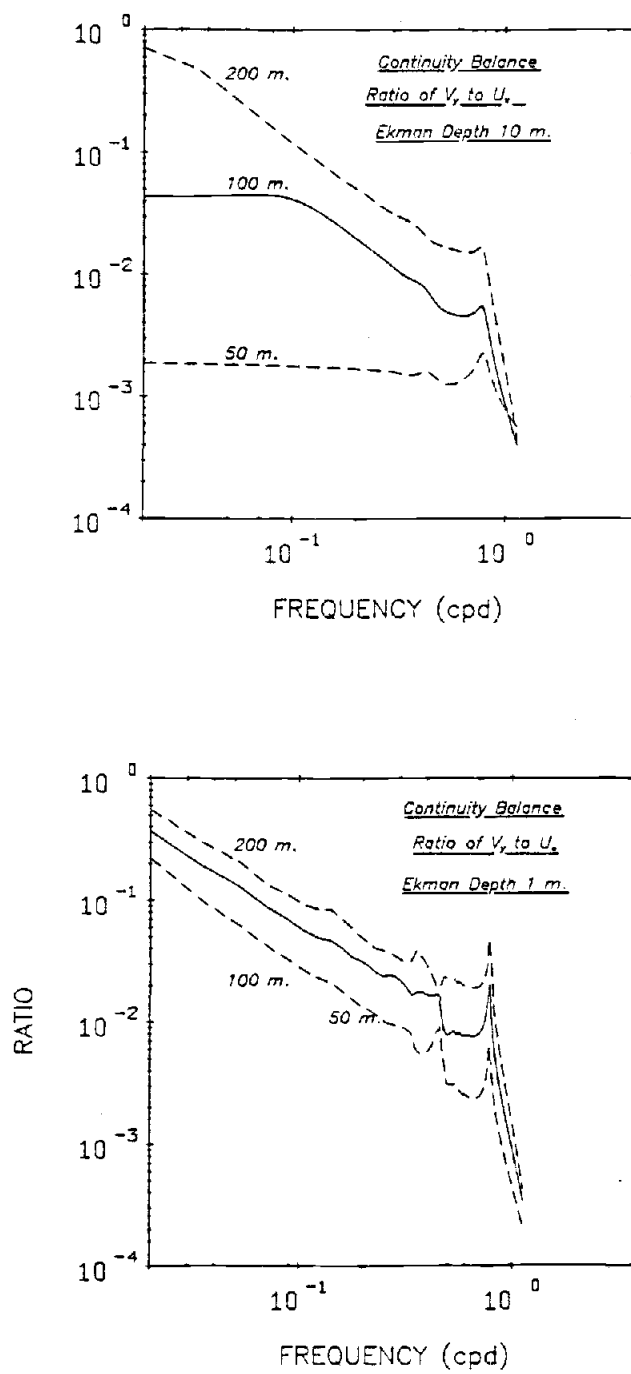


Figure 24. Balances in the continuity equation for Ekman depths of one and ten meters.

thickness. This simple mass balance is commonly assumed in upwelling models and is suggested in velocity measurements from the Oregon shelf, studied by Allen and Kundu (1978). At the 200 meter isobath the balance is essentially the same at mid-depths for both the one and ten meter cases.

In long wave models of continental shelf response the term  $U_t$  in the momentum equation (2) is frequently neglected based on scale arguments (Allen, 1980). Measurements confirm that for the inviscid interior the alongshore velocity is indeed in approximate geostrophic balance (Allen and Kundu, 1978). The alongshore momentum equation (3), on the other hand, is ageostrophic with  $V_t$  and  $fU$  having comparable magnitudes.

In this viscous model the long wave approximation is not made and the offshore and alongshore directions are assigned the same length scales. It is interesting then to compare the terms in the momentum balances, as measured by their responses. In Figure 25 the ratio of  $U_t$  to  $fV$  and of  $V_t$  to  $fU$  are drawn for mid-depths at the 50, 100 and 200 meter isobaths.

For the onshore momentum equation the neglect of  $U_t$  relative to  $fV$  is seen to be justified over much of the subinertial frequency range. The local acceleration becomes important only for time scales close to one day. The result is essentially the same for both Ekman depths of one and of ten meters and applies across the range of shelf depths.

Figure 25 also shows that in the alongshore momentum balance the

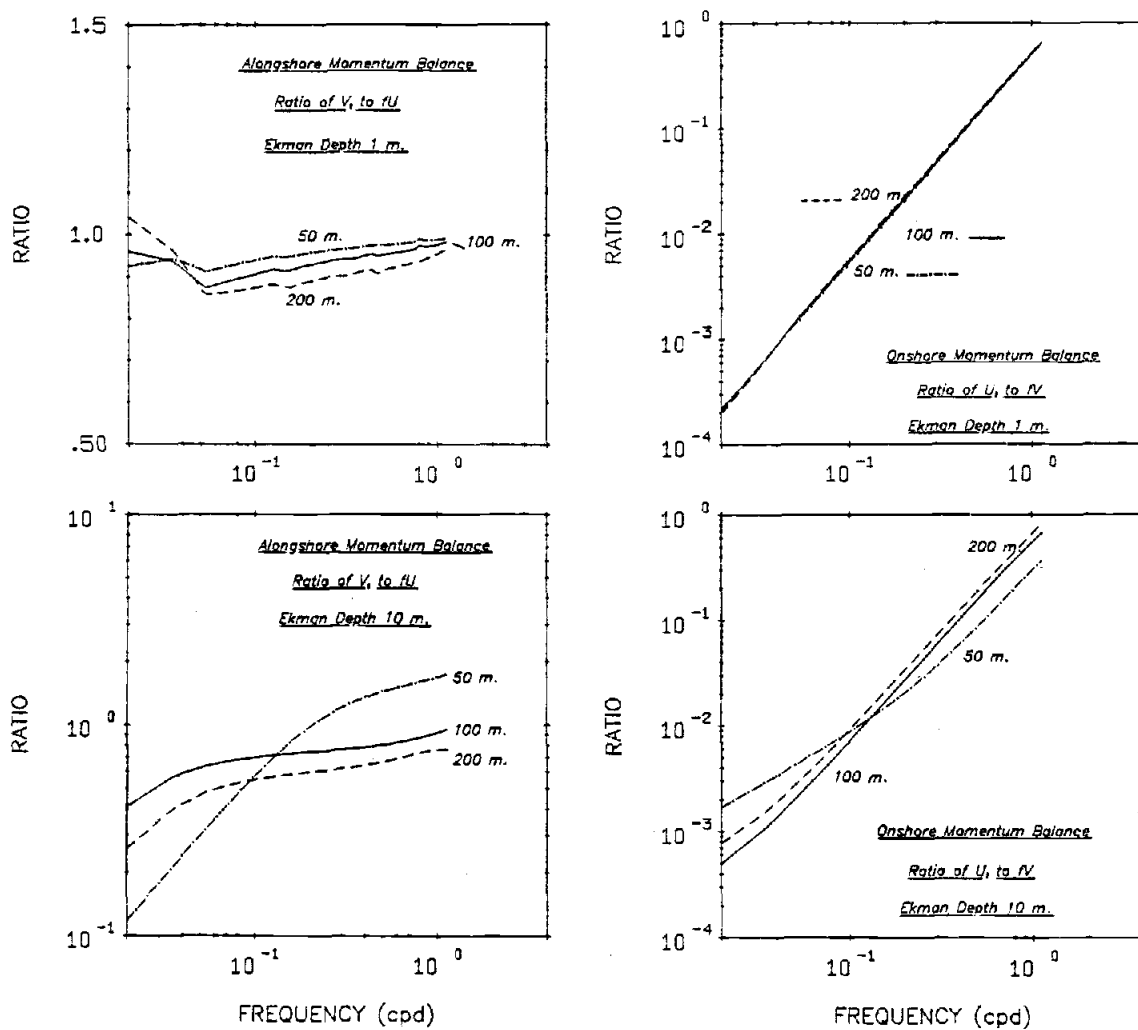


Figure 25. Balances in the horizontal momentum equations for Ekman depths of one and ten meters.

terms  $V_t$  and  $fU$  are indeed of comparable magnitude. At low frequencies for the ten meter Ekman layer thickness  $V_t$  is smallest relative to  $fU$ . Its importance increases at the higher subinertial frequencies, particularly inshore where it exceeds  $fU$  for time scales shorter than about three days. With an Ekman depth of one meter the terms are in approximate balance for the entire subinertial band.

## V. SUMMARY AND CONCLUSIONS

This study has examined the role of eddy diffusion in a non-stratified model of forced shelf circulation. Using linear Ekman dynamics the results of the previous chapter indicate that the model can account for a major part of the subinertial variance of the Oregon shelf response. With ten meter Ekman layers, which are of the expected thickness (Kundu, 1977), reasonable predictions result, both in amplitude and phase, for the coherent responses of coastal sea-level and horizontal currents to alongshore wind stress forcing. For the adjusted coastal sealevel the winter and summer responses are the same, despite the reversal of the wind stress curl (Nelson, 1976) and the seasonal cycle in atmospheric pressure fluctuations. The alongshore component of wind stress is apparently the dominant forcing agent and the response to atmospheric pressure is isostatic, at least on the Oregon shelf.

That the observed response amplitudes are consistently higher than model predictions may be partially due to the wind stress, measured at the coast, underestimating the open shelf value, as is suggested in the historical data compiled by Nelson (1976). The discrepancy is greatest for coastal sealevel, measured within Yaquina Bay. The response of sea surface elevation would perhaps be better represented by bottom pressure sensors over the shelf. Harbor effects, such as the wave set-up discussed by Thompson (1980) may have caused an over-response. The model prediction of coastal sea-level amplitude is also sensitive to the details of the nearshore

topography. The agreement of observed and model predicted phase relations is well within observational uncertainties.

The success of the model lends credence to its other features. The transfer functions that may be defined when the forcing is assumed invariant across the shelf allow a useful and convenient discussion of the properties of the model, independent of the wavenumber-frequency characteristics of a particular forcing field. Diffusion is parameterized with surface and bottom boundary layers of finite thickness, which may interact in a shallow nearshore region. The model response is found to be insensitive to the choice of nearshore boundary condition (regularity or no-flow), provided the coastal wall height, if employed, is less than the Ekman depth necessary to parameterize the effect of diffusion. This requirement has not often been imposed in the literature where topographic profiles with large coastal walls are commonly used.

The model provides an explanation for the banded structure that the coherence, between wind stress and the coastal response, is often found to exhibit (Brooks, 1978). Free waves, whose presence is expected to reduce such coherence, suffer increased attenuation in the vicinity of the cut-off frequencies of the various shelf wave modes, with a consequent enhancement of coherence for the locally forced response at such frequencies.

The balances of the continuity and momentum equations, predicted by the model, are in agreement with observation (Allen and Kundu, 1978). The mass balance becomes increasingly two dimensional as the



coast is approached, as is commonly assumed in theories of coastal upwelling. The alongshore velocity component is in geostrophic balance over most of the subinertial frequency band, while the alongshore momentum equation is ageostrophic. Across shelf phase variations, with fluctuations nearshore leading those offshore, as seen in shelf measurements also appear in the model. Another feature of the model (which could not be implemented with the present data base) is that it predicts a relationship between the wind coherent spectra of the vertical and onshore components of velocity. If the spectrum of the latter could be extricated from the noise which often contaminates it, this model result would allow the upwelling spectrum to be estimated.

Future applications of the model should include the computation of the trajectories of water parcels in response to the passage of a sequence of storm systems. The variance of alongshore wind stress has an alongshore structure, presumably the result of the distribution of storm tracks, and the influence of such spatial non-stationarity should also be considered. Another useful extension would be the inclusion of baroclinic effects. The Oregon hydrographic regime has a marked seasonal cycle (Huyer, 1977) and while the long term response appears largely barotropic, a consideration of the influence of such features as the upwelling front would be useful. An extension of the model to the two-layer case was considered but a realistic treatment, with the interface surfacing as a front or intersecting a sloping bottom, cannot be easily

encompassed with the present numerical scheme. The author hopes to consider these problems further in the future.

## BIBLIOGRAPHY

- Abramowitz, M. and I. A. Stegun, 1965. Handbook of mathematical functions. Dover, New York. 1046 p.
- Adams, J. K. and V. T. Buchwald, 1969. The generation of continental shelf waves. *J. Fluid Mech.*, 35:815-826.
- Allen, J. S., 1980. Models of wind-driven currents on the continental shelf. *Ann. Rev. Fluid Mech.*, 12:389-433.
- Allen, J. S. and P. K. Kundu, 1978. On the momentum vorticity and mass balance on the Oregon shelf. *J. Phys. Oceanogr.*, 8:13-27.
- Allen, J. S. and R. D. Romea, 1980. On coastal trapped waves at low latitudes in a stratified ocean. *J. Fluid Mech.* (submitted)
- Bakun, A., 1973. Coastal upwelling indices, West coast of North America, 1946-71. U.S. Dept. Commer., NOAA Tech. Rep. NMFS SSRF-671. 103 p.
- Bendat, J. S., and A. G. Piersol, 1971. Random data: Analysis and measurement procedures. Wiley-Interscience, New York. 407 p.
- Brink, K. H. and J. S. Allen, 1978. On the effect of bottom friction on barotropic motion over the continental shelf. *J. Phys. Oceanogr.*, 8:919-922.
- Brink, K. H., J. S. Allen and R. L. Smith, 1978. A study of low-frequency fluctuations near the Peru coast. *J. Phys. Oceanogr.*, 8:1025-1041.
- Brooks, D. A., 1978. Subtidal sealevel fluctuations and their relation to atmospheric forcing along the North Carolina coast. *J. Phys. Oceanogr.*, 8:481-493.
- Caldwell, D. R., D. L. Cutchin and M. S. Longuet-Higgins, 1972. Some model experiments on continental shelf waves. *J. Mar. Res.*, 30:39-55.
- Carrier, G. F. and H. P. Greenspan, 1958. Water waves of finite amplitude on a sloping beach. *J. Fluid Mech.*, 4:97-109.
- Frankignoul, C. and P. Muller, 1979. Quasi-geostrophic response of an infinite  $\beta$ -plane ocean to stochastic forcing by the atmosphere. *J. Phys. Oceanogr.*, 9:104-127.
- Frye, D. E., 1972. An examination of the spectrum for coastal winds on the mesoscale. M.S. thesis, Oregon State University, 53 p.

- Gilbert, W. E., A. Huyer, E. D. Barton and R. L. Smith, 1976. Physical Oceanographic observations off the Oregon coast, 1975:WISP and UP-75. Data Rep. 64, Ref. 76-4. School of Oceanogr., Oregon State University. 189 p.
- Gill, A. E. and E. H. Schumann, 1974. The generation of long shelf waves by the wind. *J. Phys. Oceanogr.*, 4:83-90.
- Halpern, D., 1974. Summertime surface diurnal period winds measured over an upwelling region near the Oregon coast. *J. Geophys. Res.*, 79:2223-2230.
- Hsiueh, Y. and C. Y. Peng, 1978. A diagnostic model of continental shelf circulation. *J. Geophys. Res.*, 83:3033-3041.
- Huthnance, J. M., 1975. On trapped waves over a continental shelf. *J. Fluid Mech.*, 69:689-704.
- Huyer, A., 1977. Seasonal variation in temperature, salinity and density over the continental shelf off Oregon. *Limnology and Oceanogr.*, 22:442-453.
- Julian, P. R. and A. K. Cline, 1974. The direct estimation of spatial wavenumber spectra of atmospheric variables. *J. Atmos. Sci.*, 31:1526-1539.
- Kraichnan, R. H., 1967. Inertial ranges in two-dimensional turbulence. *J. Phys. Fluids*, 10:1417-1423.
- Kroll, J. and P. P. Niiler, 1976. The transmission and decay of barotropic Rossby waves incident on a continental shelf. *J. Phys. Oceanogr.*, 6:432-450.
- Kundu, P. K. 1977. On the importance of friction in two typical continental waters: off Oregon and Spanish Sahara. In: J. C. J. Nihoul (editor). *Bottom Turbulence*. Elsevier, Amsterdam. 8th Liege Colloq. Ocean Hydrodyn., 1976, pp. 187-207.
- Kundu, P. K., J. S. Allen and R. L. Smith, 1975. Modal decomposition of the velocity field near the Oregon coast. *J. Phys. Oceanogr.*, 5:683-704.
- LeBlond, P. H. and L. A. Mysak, 1977. Trapped coastal waves and their role in shelf dynamics. In: E. Goldberg, I. McCave, J. O'Brien and J. Steele (Editors). *The Sea*. Wiley-Interscience, New York, 6:459-495.
- Lindzen, R. S. and H. L. Kuo, 1969. A reliable method for the numerical integration of a large class of ordinary and partial differential equations. *Mon. Weather Rev.* 97:732-734.

- Longuet-Higgins, M. S., 1968a. On the trapping of waves along a discontinuity of depth in a rotating ocean. *J. Fluid Mech.*, 31:417-434.
- Longuet-Higgins, M. S., 1968b. Double Kelvin waves with continuous depth profiles. *J. Fluid Mech.*, 34:49-80.
- Mofjeld, H. O., 1980. Effects of viscosity on Kelvin waves. (Submitted to *J. Phys. Oceanogr.*)
- Munk, W. H. and D. E. Cartwright, 1966. Tidal spectroscopy and prediction. *Philos. Trans. R. Soc. London. A* 259:533-581.
- Mysak, L. A., 1967. On the very low frequency spectrum of sealevel on a continental shelf. *J. Geophys. Res.*, 72:3043-3047.
- Mysak, L. A., 1980. Recent advances in shelf wave dynamics. *Rev. Geophys. and Space Physics*, 18:211-241.
- Nelson, C. S., 1976. Wind stress and wind stress curl over the California current. M. S. thesis. Naval Postgraduate School, Monterey, California. 136 p.
- Odulo, A. B., 1975. Propagation of long waves in a rotating basin of variable depth. *Okeanologiya*, 15:11-14.
- Pillsbury, R. D., J. S. Bottero, R. E. Still and W. E. Gilbert, 1974a. A compilation of observations from moored current meters, vol. 6, Oregon continental shelf, April-October, 1972. Data Report 57, Ref. 74-2, Sch. of Oceanogr., Oregon State University. 230 p.
- Pillsbury, R. D., J. S. Bottero, R. E. Still and W. E. Gilbert, 1974b. A compilation of observations from moored current meters, vol. 7. Oregon continental shelf, July to August 1973. Data Rep. 58, Ref. 74-7. Sch. of Oceanogr., Oregon State University. 87 p.
- Romea, R. D. and J. S. Allen, 1980. On forced coastal trapped waves at low latitudes in a stratified ocean. (Private communication)
- Smith, J. D. and C. E. Long, 1976. The effect of turning in the bottom boundary layer on continental shelf sediment transport. *Mem. Soc. R. Sci. Liege. be ser.*, tome x. pp. 369-396.
- Sobey, E. J. C., 1977. The response of Oregon shelf waters to wind fluctuations: differences and the transition between winter and summer. Ph.D. thesis, Oregon State University, 153 p.

- Thompson, R. O. R. Y. and B. V. Hamon, 1980. Wave setup of harbor water levels. *J. Geophys. Res.*, 85:1151-1152.
- Wang, D. P., 1976. Coastal water response to the variable wind: theory and coastal upwelling experiment. Tech. Rep. TR76-2, Rosenstiel Sch. of Marine and Atmospheric Sci., University of Miami. 174 p.
- Willebrand, J., 1978. Temporal and spatial scales of the wind field over the North Pacific and North Atlantic. *J. Phys. Oceanogr.*, 8:1080-1094.

## APPENDICES

Appendix A: The Regularity Condition

Suppose the nearshore topography is linear

$$H(x) = mx$$

where  $m$  is the bottom slope. Using the series expansions for the hyperbolic tangent and secant (Abramowitz and Stegun, 1965) the complex functions of equation (14) are written as

$$h(x) = \sum_{j=3}^{\infty} h_j x^j$$

$$H(x) = \sum_{j=5}^{\infty} H_j x^j$$

$$\frac{1-\sigma^2}{2\mu\sigma} \{(\phi_\beta - \phi_\alpha) x + \lambda(\phi_\beta + \phi_\alpha)\} = \sum_{j=2}^{\infty} r_j x^j$$

Here

$$h_j = \begin{cases} 0 & , j \text{ even} \\ m^j t_j \left\{ \frac{1-\sigma}{2\sigma} \beta^{j-1} - \frac{1+\sigma}{2\sigma} \alpha^{j-1} \right\} & , j \text{ odd} \end{cases}$$

$$H_j = \begin{cases} 0 & , j \text{ even} \\ -m^j t_j \left\{ \frac{1-\sigma}{2} \beta^{j-1} + \frac{1+\sigma}{2} \alpha^{j-1} \right\} & , j \text{ odd} \end{cases}$$

$$r_j = \begin{cases} K\lambda m^j s_j (\beta^{j-2} + \alpha^{j-2}) & , j \text{ even} \\ K(j+1)m^{j+1} s_{j+1} (\beta^{j-1} - \alpha^{j-1}) & , j \text{ odd} \end{cases}$$

with

$$K = \frac{1-\sigma^2}{2\mu\sigma}$$

and



$$t_{2n-1} = 2^{2n} (2^{2n} - 1) B_{2n} / (2n)!$$

$$s_{2n} = -E_{2n} / (2n)!$$

$B_{2n}$  and  $E_{2n}$  are the Bernoulli and Euler numbers respectively.

If we now define

$$c_{nj} = \lambda^2 h_{n-j+1} - j(n+2)h_{n-j+3} - \frac{\lambda}{\sigma}(n-j+2)H_{n-j+2}$$

the coefficients  $(a_n, b_n)$  of the series expansions necessary for the evaluation of the regular boundary condition obey the following recurrence relations

$$a_n = \{r_{n+1} + \sum_{j=1}^{n-1} c_{nj} a_j\} / n(n+2)h_3$$

$$b_n = \{\lambda^2 h_{n+1} - \frac{\lambda}{\sigma}(n+2) H_{n+2} + \sum_{j=1}^{n-1} c_{nj} b_j\} / n(n+2)h_3$$

with

$$a_1 = r_2/3h_3 \quad , \quad b_1 = 0.$$

### Appendix B: The Stationarity Test

Estimates of spectral density are computed from

$$S_n = \frac{1}{2} T (a_n^2 + b_n^2)$$

where  $T$  is the record duration. The raw Fourier components  $(a_n, b_n)$  at each frequency are assumed to have independent normal distributions with mean zero and population variance  $\sigma^2$ . Hence, the quantity

$$\left( \frac{2}{T\sigma^2} \right) S_n \quad (B1)$$

should be distributed as  $\chi^2_2$ . Likewise, if we ensemble average over  $N$  segments of equal duration, the quantity

$$\frac{2}{T\sigma^2} \sum_{i=1}^N (S_n)_i \quad (B2)$$

should have a  $\chi^2_{2n}$  distribution. The ratio of (B1) to (B2) will then be distributed as  $F_{2,2n}$ . This ratio is simply

$$S_n / \bar{S}_n$$

where  $\bar{S}_n$  is the sample mean of the spectral density drawn from the  $N$  estimates. For each frequency the spectral estimates normalized by their sample mean are tested for goodness of fit to the  $F_{2,2n}$  distribution.

This is done with a  $\chi^2$  test. The  $N$  values are divided into  $m$  equiprobable categories. If the observed and expected frequencies are denoted by  $O_j$  and  $E_j$ , then

$$\chi^2 = \sum_{j=1}^m (O_j - E_j)^2 / E_j$$

is evaluated and compared to the  $\chi^2_{m-1}$  distribution.

The degree of stationarity may be expressed in terms of the Type I error. This is the probability of error if the hypothesis of stationarity is rejected. A low value of Type I error is associated with a high degree of non-stationarity.